10-23-2019

Cross-Linked Polyphenol-Based Drug Nano-Self-Assemblies Engineered to Blockade Prostate Cancer Senescence

Prashanth K.B. Nagesh

Pallabita Chowdhury

Elham Hatami

Sonam Kumari

Vivek K. Kashyap

See next page for additional authors

Authors

Prashanth K.B. Nagesh, Pallabita Chowdhury, Elham Hatami, Sonam Kumari, Vivek K. Kashyap, Manish Tripathi, Santosh Wagh, Bernd Meibohm, Subhash C. Chauhan, Meena Jaggi, and Murali M. Yallapu

HHS Public Access

Author manuscript

ACS Appl Mater Interfaces. Author manuscript; available in PMC 2021 April 05.

Published in final edited form as:

ACS Appl Mater Interfaces. 2019 October 23; 11(42): 38537–38554. doi:10.1021/acsami.9b14738.

Cross-Linked Polyphenol-Based Drug Nano-Self-Assemblies Engineered to Blockade Prostate Cancer Senescence

Prashanth K.B. Nagesh[†,‡], **Pallabita Chowdhury**[‡], **Elham Hatami**[‡], **Sonam Kumari**[‡], **Vivek Kumar Kashyap**[†,‡], **Manish K. Tripathi**[†,‡], **Santosh Wagh**[‡], **Bernd Meibohm**[‡], **Subhash C. Chauhan**[†,‡], **Meena Jaggi**[†,‡], **Murali M. Yallapu**[*,†,‡]

[†]Department of Microbiology and Immunology, School of Medicine, University of Texas Rio Grande Valley, McAllen, Texas 78504, United States

[‡]Department of Pharmaceutical Sciences and Center for Cancer Research, University of Tennessee Health Science Center, Memphis, Tennessee 38163, United States

Abstract

Cellular senescence is one of the prevailing issues in cancer therapeutics that promotes cancer relapse, chemoresistance, and recurrence. Patients undergoing persistent chemotherapy often develop drug-induced senescence. Docetaxel, an FDA-approved treatment for prostate cancer, is known to induce cellular senescence which often limits the overall survival of patients. Strategic therapies that counter the cellular and drug-induced senescence are an unmet clinical need. Towards this an effort was made to develop a novel therapeutic strategy that targets and removes senescent cells from the tumors, we developed a nanoformulation of tannic acid−docetaxel self-assemblies (DSAs). The construction of DSAs was confirmed through particle size measurements, spectroscopy, thermal, and biocompatibility studies. This formulation exhibited enhanced *in vitro* therapeutic activity in various biological functional assays with respect to native docetaxel treatments. Microarray and immunoblot analysis results demonstrated that DSAs exposure selectively deregulated senescence associated TGFβR1/FOXO1/p21 signaling. Decrease in β-galactosidase staining further suggested reversion of drug-induced senescence after DSAs exposure. Additionally, DSAs induced profound cell death by activation of apoptotic signaling through bypassing senescence. Furthermore, *in vivo* and *ex vivo* imaging analysis demonstrated the tumor targeting behavior of DSAs in mice bearing PC-3 xenograft tumors. The antisenescence and anticancer activity of DSAs was further shown *in vivo* by inhibiting TGFβR1 proteins and

[*]**Corresponding Author** Mailing address: Department of Immunology and Microbiology, 5300 North L Street, Room 2.249, McAllen, TX 78504. Phone: (956) 296-1705. Fax No: (956)-296-1325. murali.yallapu@utrgv.edu.

Author Contributions

P.K.B.N designed, performed, and analyzed data and wrote the paper. P.C., E.H., S.K., V.K.K., and S.W. performed experiments. B.M. provided instrumentation facilities. M.K.T. was involved in curating and analyzing *ONCOMINE* data and figure preparation. P.C. participated in method section writing and manuscript editing. M.M.Y and P.K.B.N conceived the idea and analyzed data and were crucially involved throughout the study. M.M.Y., S.C.C., and M.J. critically evaluated data, participated in discussion of results, and edited and reviewed the manuscript.

ASSOCIATED CONTENT

Supporting Information

The Supporting Information is available free of charge on the ACS Publications website at DOI: 10.1021/acsami.9b14738.

Results; hemolysis studies of DSAs; LC-MS/MS studies of DSAs; *ONCOMINE* data analysis; androgen deprivation status of the ONCOMINE data sets iPathwayGuide analysis of DSAs (PDF)

The authors declare no competing financial interest.

regressing tumor growth through apoptotic induction in the PC-3 xenograft mouse model. Overall, DSAs exhibited such advanced features due to a natural compound in the formulation as a matrix/binder for docetaxel. Overall, DSAs showed superior tumor targeting and improved cellular internalization, promoting docetaxel efficacy. These findings may have great implications in prostate cancer therapy.

Graphical Abstract

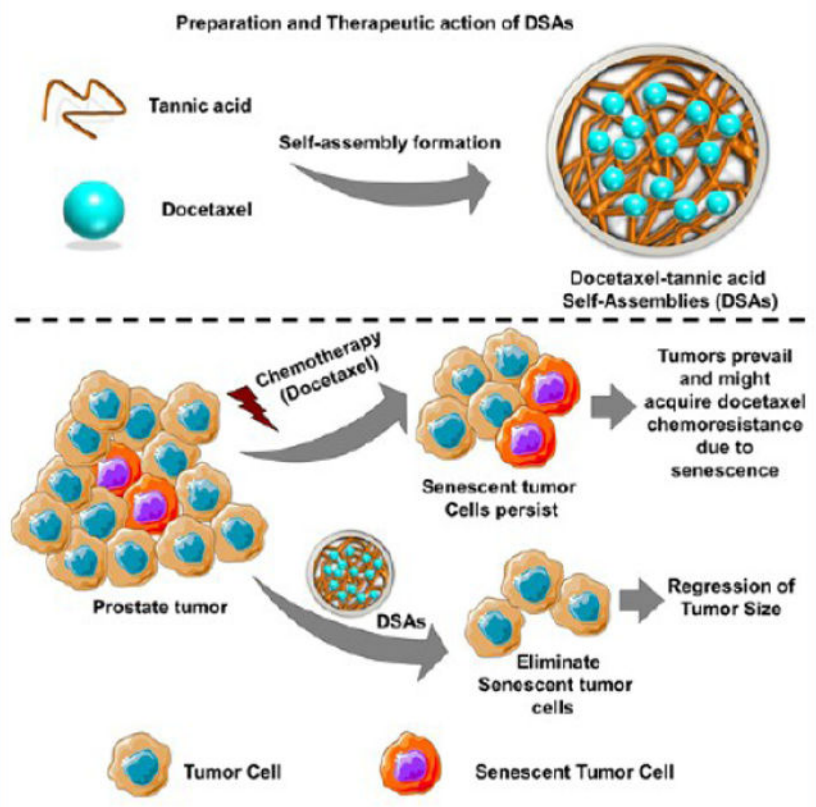

Keywords

prostate cancer; senescence; nanoassemblies; docetaxel; DSAs; apoptosis

INTRODUCTION

Prostate cancer is the most commonly diagnosed cancer with 174 650 new cases (20% of all male cancers) and accounts for 31 620 deaths (10% of all male cancers) in the United States.[1] There are no significant beneficial standard chemotherapeutic options available in patients after androgen deprivation therapy.[2] In spite of advances in therapeutic modalities against prostate cancer, the survival rates in patients have improved by meager months.[3] Taxanes are the most propitious class of drugs with durable anticancer properties. Docetaxel (Dtxl), a second generation taxane family drug, revealed promising survival benefits in prostate cancer patients. Docetaxel increased survival up to 25 months leading to its subsequent approval by the Food and Drug Administration (FDA) in 2010.[4] Unfortunately, the majority

of patients acquire resistance to treatment with Dtxl within 12 months from the start of therapy. This leads to the propagation of the disease and remains a challenging task in clinics.[5] Two pivotal mechanisms that favor resistance toward Dtxl treatment are the expression of the multidrug resistance (MDR) phenotype and alterations in the tubulin system.[6] Aberrations in the signaling pathways that alter the cell cycle and apoptotic regulation[7] are another putative mechanism of resistance. Chemoresistance commences during therapies due to the activation of intracellular DNA repair mechanism resulting in the culmination of apoptosis or growth arrest.[8] Such resistant cells activate alternative survival mechanisms called “senescence”.

Cellular senescence is defined as a state of irreversible growth arrest that is elicited due to chemotherapy stress.[9] This phenomenon is characterized by senescence-associated β-galactosidase (SA-β-gal) activity, telomere shortening, secretion of cytokines, chemokines, and proteases. Senescence is a cumulative stimulation of many signaling pathways that also include activation of TGFβR1/FOXO1/p21 that simultaneously regulate the cell proliferation rates of the cancer cells.[10] The physiological events such as immune mediated attrition[11] and sustained *in vivo* accumulation of senescent cells[12] could provide a potential repository for cancer relapse and chemoresistance.[8] Preclinical and clinical studies have evidently clarified that docetaxel treatment can cause chemoresistance through senescence mechanisms in prostate cancer.[13] Targeting senescent cells during Dtxl treatments is an unmet clinical need. Thus, the aim of our study was to develop a strategy that can tackle the senescence. To eliminate senescent cells from the tumors advanced therapeutic strategies need to be implemented. A nanoparticle (NP) therapeutic strategy can be enabled to target and eradicate cells expressing the senescence associated secretory phenotype (SASP).[14] Nanoparticle technology can offer great benefits for delivery of therapeutics by overcoming the limitations exist in current conventional chemotherapy.[15] A variety of nanoparticle based carriers varying in size from 1 to 1000 nm include polymeric nanoparticles, dendrimers, liposomes, inorganic materials (metal nanoparticles or quantum dots), and biological materials (viral nanoparticles or albumin nanoparticles) have been applied in nanomedicine research.[16] Systemic clearance of the nanoparticle is necessary after the delivery of the drug to the target site and any related immunological responses need to be addressed.[17] Natural origin polyphenols have addressed the immunological concerns and can be easily degraded by systemic enzymatic activities.[18] The most beneficial aspect of these polyphenolic compound-based nanoformulations is that they exhibit chemopreventive and anticancer activity along with carrying drug entities. This offers enhanced therapeutic benefits, with reduced systemic toxicity due to the chemotherapy drugs.[19]

Tannic acid (TA), a plant-derived polyphenol has shown potential anticancer activity against various cancers, such as prostate,[20] breast,[21] bile duct,[22] and oral[23] cancers. The antitumorigenic role of TA in prostate cancer has been elucidated by our group[24,25] and other research teams.[20] TA is also known to prevent chemoresistance in cancer cells.[22] However, alone TA as an anticancer agent may not work efficiently due to the high concentrations required to act on tumors. On the other side, the delivery of Dtxl has been achieved through nanoparticulate systems previously.[26,27] However, ineffective and suboptimal therapeutic indices of the drug (Dtxl) failed in preventing the acquisition of to prevent chemoresistance and the senescence phenotype in cells, dwelling in the tumor

microenvironment.[28–31] To combat the shortcomings of Dtxl, we formulated a novel tannic acid based Dtxl nano-self-assembly for treatment against prostate cancer. TA can assist the solubilization of docetaxel and form self-assemblies through hydrogen or ionic bonding.[32] The docetaxel−tannic acid self-assemblis (DSAs) based nanoparticle strategy has proven to be an efficient delivery method to transport docetaxel to prostate cancer cells and xenograft tumors and block cellular senescence. The obtained results demonstrate the superior anticancer activity of DSAs and inhibition of the senescence blockade in the prostate cells and tumors. We believe that this is the first report to demonstrate the targeting of prostate cancer senescence by a nanoformulation approach leading to the inhibition of SASP associated signaling in prostate cancer.

MATERIALS AND METHODS

Materials.

All laboratory reagents, solvents, and chemicals were purchased from Sigma-Aldrich Co. (St. Louis, MO, USA) or Fisher Scientific (Pittsburgh, PA, USA) and were used without any further purification. Docetaxel (98% purity) was purchased from Acros organics (Hampton, NH, USA). All cell culture plastics were purchased from Sarstedt, Inc. (Newton, NC, USA).

Cell Culture, Growth Conditions, and Treatment.

Cell lines of prostate cancer (C4-2, DU145, and PC-3) were obtained from American Type Culture Collection (Manassas, VA, USA). All these frozen cell lines were revived and cultured under aseptic conditions for all experiments. The cell lines were maintained in Rosewell Park Memorial Institute 1640 (RPMI) or Dulbecco's Modified Eagle Medium (DMEM) and supplemented with 10% heat-inactivated fetal bovine serum (Thermo Fisher Scientific), D-glucose (2 g/L), L-glutamine with other amino acids, and 1% antibiotic-antimycotic (Thermo Fisher Scientific, Waltham, MA, USA) at 37 °C in a humidified atmosphere (5% CO_2 and 95% O_2, ThermoScientific, Waltham, USA). For all cell culture studies, cell lines were trypsinized and monodispersed suspensions were plated and allowed to adhere for overnight before initialization of treatments. Early passage cells were used for all of our experiments.

Preparation of DSAs.

The docetaxel self-assembly formation was achieved by a solvent evaporation method (Figure 1A) as described earlier.[33] For this, 5 mg of tannic acid (MW 1701.19 g/mol, ACS reagent grade) was dissolved in 1 mL milli-Q water containing 8 mL glass vial. To this solution, 100 μL of Dtxl in acetone (1 mg/mL) was added dropwise and this mixture was stirred at a speed of 900 rpm (Benchmark digital magnetic hot plate stirrer, ABC Scientific, Glendale, CA, USA). The DSA formation results upon acetone evaporation. Three cycles of extrusion were applied and centrifuged at 2000 rpm (Sorvall ST 8 Centrifuge, Thermo Fisher Scientific, Suzhou, China) to remove the larger clusters and unbound Dtxl. Docetaxel in DSAs was estimated using the LC-MS/MS method.[34]

Physico-chemical and Hemocompatibility Characterization of DSAs.

In order to characterize the docetaxel nanoassemblies, various techniques such as dynamic light scattering (DLS), transmission electron microscopy (TEM), Fourier transform infrared spectroscopy (FT-IR), X-ray diffraction (XRD), and thermogravimetric analysis (TGA) were used.

The size of the particle and its distribution and zeta potential of the DSAs were measured using a NanoZS Zetasizer dynamic light scattering (DLS) (Malvern Instruments Ltd., Malvern, UK) system with a 633 nm red laser at 90° angle. For these measurements, 50 μL of 1 mg/mL DSAs solutions were dispersed in 1 mL milli-Q water in a disposable cuvette (Sarstedt Inc., Newton, NC) and subjected for sonication (30 s and four pulses) (VirSonic Ultrasonic Cell Disrupter 100, VirTis, Woburn, MA, USA). The DLS measurements were performed for 3 min to record intensity average cumulative diameter and distribution of particle size. To investigate the surface charge of the DSAs, typical Zeta potential (ζ, mV) measurements (60 runs) were conducted (triplicate measurements, 20 runs each time) in 1X PBS solutions via a laser Doppler velocimetry method.[33]

The particle morphology (shape and size) of DSAs was investigated by JEOL 200EX transmission electron microscope (JEOL Ltd., Tokyo, Japan) using an AMT camera (100 000×) operating at 80 kV. About 100 μL of DSAs suspension was deposited on the shiny side of a 150 mesh copper grid (Electron Microscopy Sciences, Hatfield, USA), and these air-dried nanoparticles were imaged.[33]

The crystalline behavior of the DSAs was determined by X-ray measurements on a Rigaku D/Max-B diffractometer (Rigaku Americas Corp, Woodlands, TX, USA) using Cu−Kα radiation.[33] FT-IR measurements were acquired using PerkinElmer Series Spectra 100 (PerkinElmer, Waltham, MA) on the attenuated total reflection objective at a scanning speed of 2 cm^{-1}. The spectral data (4000−650 cm^{-1}) was reported as an average data of 16 scans. [33] Thermal analyses were carried out on a Q50 thermogravimetric analyzer (TA Instruments, New Castle, DE, USA) under dry nitrogen atmosphere at a flow rate of 10 °C/min ranging from 50 to 500 °C.[33] Note: Lyophilized DSAs samples (FreeZone, Labconco, Kansas City, USA) were used for X-RD, FT-IR, and TGA characterization.

The hemocompatibility of DSAs was performed using hemolytic assay as described previously.[33] A freshly collected healthy male whole blood sample (1 mL) in heparinized tube (Interstate Blood Bank, Inc., Memphis, TN, USA) was centrifuged at 1000 rpm for 5 min. The supernatant was discarded, and the erythrocyte pellet was washed with normal saline to remove lysed hemoglobin. This healthy erythrocyte population was diluted to 8 mL using 1X PBS solution. Various concentrations 0.1−100 μg docetaxel in DMSO or 0.1−100 μg docetaxel equivalent DSAs were incubated with 200 μL of erythrocyte suspension for 2 h at 37 °C. Sodium dodecyl sulfate (1 mg/mL PBS solution) or water served as a positive control (100% lysis) while PBS solution acted as a negative control (0% lysis) in this assay. The extent of hemolysis is confirmed by the hemoglobin release into the solution which will be collected as a supernatant by centrifuging at 1000 rpm for 5 min at 4 °C. The hemoglobin in suspension was measured from the absorbance at 490 nm using Cytation 5 (BioTek Instruments, Inc., Winooski, VT, USA). The percent hemolysis was calculated using the

following equation: % hemolysis = [(abs of sample − abs of negative control)/(abs of positive control − abs of negative control)] × 100. From this study, aliquots of erythrocytes were smeared on a glass slide and the structural morphology of erythrocytes was captured using a microscope (EVOS FL Cell Imaging System, Carlsbad, CA, USA).

Intracellular Drug Uptake.

Intracellular drug accumulation of docetaxel and DSAs inside the PC-3 was determined using liquid chromatography-tandem mass spectrometry (LC-MS/MS) following our earlier report.[33] For this, 60−70% confluent grown cells in 100 mm dishes were treated with 500 nM Dtxl/DSAs for 1, 2, and 6 h. Untreated cells and cells treated with plain TA served as the experimental control(s). Cell pellets were collected after treatment by trypsinization and centrifuging at 1000 rpm (Thermofisher, Waltham, USA) for 5 min. To extract the internalized drug, the cell pellet was resuspended in CelLytic M buffer with intermittent sonication (Ultrasonic Homogenizer, Biologics, Inc., Manassas, VA, USA), for 5 min durations at 200 W, in an ice bath. A liquid LC-MS/MS using an LC system (Shimadzu Corporation, Kyoto, Japan) connected to a Triple Quad 5500 tandem mass spectrometer (AB SCIEX, Framingham, MA) and XTerra MS C18 Column Reversed-Phase 3.5 μm Spherical Hybrid, 4.6 mm × 50 mm (no. 186000432, Waters, Milford, MA) were utilized to determine internalized drug in cells. The detailed method was presented in our previously published work.[33] In this method, under a flow rate of 0.8 mL/min Dtxl was eluted at a retention time of 2.28 min. Paclitaxel (Ptxl) served as the internal standard. Analytes were quantified using multiple reaction monitoring to monitor the ion transitions of m/z of 830.4 → 549.2 for DTX and m/z 876.5 → 308.30 for Ptxl. The calibration standards were prepared in CelLytic M (C2978), and the range of linear response of Ptxl was 2.44−5000 ng/mL with R^2 = 0.99475.

Cell Proliferation Assay.

The superior antiproliferative effects of the DSAs was evaluated by MTS assay in prostate cancer (C4–2, DU145, and PC-3) cell lines.[35,36] Briefly, 5×10^3 cells were seeded in each well of a 96-well plate (Sarstedt Inc., Newton, NC, USA) and allowed overnight cells to attach to the plate. Subsequently, cells were exposed to 1−40 nM Dtxl in DMSO solution or 1−40 nM Dtxl equivalent DSAs for 48 h. Each treatment was carried out in sextuplicate. Equivalent DMSO and TA served as vehicle and nanoparticle controls, respectively. After a treatment period, 20 μL MTS reagent (Promega, Madison, WI, USA) was supplemented on these treated cells and incubated for 2−3 h. Then the plates were read by Microplate Reader (BioTeK Cytation 3, Winooski, VT, USA) at absorbance of 490 nm. The percent cell proliferation was calculated as described previously.[35,36]

Clonogenic Formation Assay.

The clonogenic potential of the DSAs was investigated through colony formation assay.[37] C4–2 and PC-3 cell lines were seeded at a density of 250 cells/well in a 12-well plate. The cells were allowed to grow for 2−3 days until they achieve individual colonies of 4−5 cells as a group in wells. Then cells were treated with 2.5 and 5 nM Dtxl and 2.5 and 5 nM Dtxl equivalent DSAs along with control/vehicle controls for a week. After the treatments for a week, drug free medium was added to the cells, and cells were allowed to grow for an

additional week. The colonies formed were fixed using cold methanol, stained by hematoxylin, and imaged as described previously.[37]

Cellular Uptake and Endosomal Escape Studies.

The cellular uptake and fate of DSAs in C4–2, DU145, and PC-3 cells were performed by employing flow cytometry and confocal methods. For these studies, coumarin 6 (C6) was labeled to DSAs following our established method[38] to track them visually in cells. For the qualitative cellular uptake experiment, 2.5×10^5 cells/well were seeded in a 6-well plate and grown for a day. Then cells were treated with 2.5−50 μg C-6 equiv C6-DSAs for 3 h. Then, cells were rinsed with 1X PBS, trypsinized, centrifuged at 1000 rpm for 5 min, and suspended in phenol red free medium. The fluorescence in cells due to C6 or C6-DSAs were measured using flow cytometer (ACEA NovoCyte 1000, ACEA Biosciences, Inc. San Diego, Ca, USA).[39,40] For confocal uptake analysis (uptake and cellular fate of DSAs), cells (2.5×10^4 cells/well) were seeded in 4-well chambered slides and were subjected to 5 μg dye or 5.0 μg C-6 equiv C6-DSAs for 3 h. Then cells were washed, rinsed with PBS, and fixed using 2% paraformaldehyde for 20 min.[38,41] Endosomal (transferrin-early; Rab7a-Late, Thermofisher, Waltham, USA) and lysosomal (Red DND-99, Thermofisher, Waltham, USA) markers were used to localize the DSAs in cells. The cell images were captured at 40× magnification under a laser confocal microscope (Carl Zeiss LSM 710, Oberkochen, Germany).

ONCOMINE Data Evaluation.

The transcriptomic expression levels of senescence associated markers in prostate cancer were investigated using the *ONCOMINE* database (https://www.oncomine.org).[42] The expression fold of senescence markers [TGFβR1, RB1(Rb), and CDKN1A (p21)] at mRNA level in prostate cancer tissues was compared with its normal tissues was acquired.

Senescence Associated β-Galactosidase Staining.

Prostate cancer (C4–2 and PC-3) cells were seeded at a density of 2.5×10^5 cells/well in 6-wells and allowed to grow. At 70% confluency, cells were treated with 10 nM Dtxl and 10 nM Dtxl equivalent DSAs for 24 h. These cells were washed with 1X PBS, fixed with 3% formaldehyde, and then subjected to β-galactosidase activity[43] using a senescence-associated β-galactosidase (SA-β-gal) staining kit (Sigma-Aldrich, St. Louis, MO) for 24 h. In principle, the intracellular SA-β-gal activity performs the hydrolysis of the substrate moieties of x-gal (blue stain) that results the accumulation of blue color in senescence cells. Cellular images were obtained by an EVOS FL imaging system.

Western Blot Studies.

The molecular signaling effects of DSAs were evaluated by Western blot studies. C4–2 and PC-3 cells were treated with 10 nM Dtxl and DSAs for 24 h. TA (5 μg) was used as another group to compare to DSAs, and untreated group served as control. After treatment, cells were scraped and suspended protein lysis buffer supplemented with protease and phosphatase inhibitor cocktail (ThermoFisher, Waltham, MA). The proteins were extracted and performed western studies as described previously.[33]

RNA Isolation, Purification, and Micro-Array Studies.

The total RNA was isolated and extracted from the cells treated with Dtxl/DSAs using TRIzol method. This extracted RNA was purified and processed for microarray studies as described previously.[33] For gene microarray studies we employed Clariom S Human gene array chip (Affymetrix, Santa Clara, CA, USA).

Animal Studies.

Xenograft Mice Model Generation.—We investigated the *in vivo* tumor accumulation and therapeutic effects of the DSAs in prostate cancer cell line (PC-3) derived subcutaneous xenograft mouse model. All animals were housed under specific pathogen-free conditions according with the recommendation of the Association for Assessment and Accreditation of Laboratory Animal Care (AAALAC) guidelines. All animal experiments were performed in full compliance with institutional guidelines and approved by the Animal Use and Care Administrative Advisory Committee at the University of Tennessee Health Science Center. For all animal studies, 6−8-week-old athymic male nude mice (Jackson laboratory, Bar Harbor, ME USA) were chosen to generate subcutaneous xenograft tumors.[44] In brief, PC-3 cells (2×10^6/mice) were subcutaneously implanted on the dorsal flank into each animal using matrigel (Corning Inc., Corning, NY). Mice were allowed for the tumor development and tumor volumes were measured using a digital caliper and calculated tumor volumes as $V = (0.5238 \times L \times W \times H)$, where L, W, and H are length, width, and height of the tumor, respectively.

Biodistribution and Tumor Accumulation.—To investigate the biodistribution and tumor accumulation of DSAs study, tumors bearing mice (~300−500 mm^3) were utilized. This size tumors are appropriate for tumor accumulation studies because (i) smaller tumors may not give accurate accumulation patterns and (ii) bigger tumors may prevent nanoparticles from penetrating due to the excessive fibrous matrices in tumors. Mice were randomly divided into groups (4 mice per group), and one time Indocyanine green (ICG) dye (100 μg/mice in 100 μL PBS) or ICG-tagged DSAs[45] (100 μg ICG-equiv DSAs/mice in 100 μL PBS, as prepared like C6-DSAs) were intraperitoneally administered to monitor DSA distribution in mice at different time points (3, 6, 24, 48, and 72 h) using an IVIS XRMS Imaging System (Caliper Life Sciences, Waltham, MA) equipped with a coupled device camera (CCD). These mice were fed with Teklad Global Rodent Diets (Envigo, Huntingdon, United Kingdom) to avoid background fluorescence due to diet. For *in vivo* ICG/ICG-DSAs tracking and accumulation in live mice, an imaging procedure was performed after anesthetization each time with a 3% flow rate of isoflurane during the induction, and 2% during the maintenance period (scanning time). All live images of mice were acquired for ICG presence which was detected using a long-pass excitation filter at 690 nm at a fixed exposure time (5000 ms). The fluorescence signal intensity is measured in photons per second per square centimeter per steradian ($p/s \cdot cm^2 \cdot sr$). To further confirm the superior tumor accumulation of ICG-DSAs, mice were sacrificed after 72 h treatment with CO_2 exposure and cervical dislocation. Then major organs, the tumor, heart, lung, liver, kidney, and spleen, were collected, and the *ex vivo* imaging of these tissues were examined using same protocol on a Petri dish.

Antitumor and Antisenescence Effects of DSAs.—When, the tumors were grown to ~100 mm^3, the mice were randomly divided into four groups (4 mice per group) for treatment: treatment groups (Dtxl (30 mg/kg) and DSAs (equivalent to Dtxl, 30 mg/kg)) and control groups (1X PBS and TA). Treatments were administered intraperitoneally in 50 μL PBS solution, twice in a week, for 5 weeks. At the end of treatment for 5 weeks or when the tumor volumes attained 800 mm^3, mice were euthanized and tumors were excised and, then, formalin fixed and paraffin embedded. Further, the tissues were sectioned and used for immuno-histo-chemical studies.[44] Also, to confirm the *in vivo* antisenescence effects of DSAs, we conducted the *ex vivo* β-galactosidase staining of excised tumors (20 mg in wt) obtained from mice with PC-3 xenograft tumors treated with TA, Dtxl, and DSAs formulation.[46] Results are representative of two times therapy experiment (4 mice per group each time).

In Vivo Toxicity Evaluation.

After the above treatments, when all mice were euthanized, their serum samples and major organs (i.e., lungs, liver, hearts, kidneys, and spleens) were collected. Serum samples were analyzed for clinical chemistry for kidney and hepatic functions (aspartate aminotransferase (AST), alanine aminotransferase (ALT), alkaline phosphatase (ALP), total protein (TP), total bilirubin (TBili), albumin (Alb), creatinine (create), blood urea nitrogen (BUN), calcium (Ca), glucose (Glu)) by using a DiaSys Respons 910 vet chemistry analyzer (DiaSys Diagnostic Systems, USA, LLC, Wixom, MI).[47] This data was tested and compared to treated mice groups. Additionally, H&E staining of the mouse organs and erythrocytes of mouse were utilized to determine extent of systemic toxicity after docetaxel treatment and how DSAs can minimize such toxicity issues.

Immuno-histochemistry.

To affirm the *in vitro* pharmacological effects of the nanoformulation, the immuno-histochemistry (IHC) studies of the excised tumors treated with DSAs were performed as described previously.[44,48,49]

Statistical Analysis.

All data were acquired and analyzed through Graph pad Prism 5.03 Software (GraphPad Software, San Diego, CA), and results were presented as mean ± standard error of mean (SEM) because it denotes the variability of the mean within the data set. All statistical analysis was performed using student's *t* test. *P* values of <0.05, 0.01, and 0.001 were considered to represent statistically significant difference w.r.t. controls.

RESULTS

Preparation and Characterization of the DSAs.

The docetaxel self-assembled nanoparticles were prepared by the conventional solvent evaporation and extrusion method as shown in Figure 1A. The amalgamation of docetaxel in DSAs was achieved by dropwise addition of the drug (docetaxel in acetone) to tannic acid solution (5 mg/mL) and continued under vigorous stirring overnight. The evaporation of acetone favors the formation of nano self-assemblies (nanoparticles) in an aqueous

environment. Tannic acid was chosen to obtain docetaxel self-assemblies as tannic acid forms instantaneous hydrogen bonding that enables cross-linking with docetaxel molecules to form frame networks in the solution.[50] On the other hand, docetaxel molecules are dispersed on tannic acid matrices which offer stable dispersion by acting as a hydrotropic-like solubilizing agent, in an aqueous environment. Larger aggregates are removed by quick spinning of formulation at 2000 rpm for 5 min. The DSAs exhibited 95.42 μg of Dtxl for 1 mg of TA containing formulation. This leads to an encapsulation efficiency of ~95%. This range of drug encapsulation was observed even with our earlier reported for TA based paclitaxel nanoparticles (96.49 ± 0.43%).[33] The particle size, particle size distribution, surface charge, chemical composition, physical, thermal, and hemocompatibility properties of resultant nanoparticle self-assemblies were characterized using DLS, FT-IR, X-RD, TGA, and hemolysis methods, respectively.

The average particle size of DSAs in water was found to be 87.78 ± 1.91 nm. A modest change in their particle size i.e., 85.02 ± 7.24 and 124.13 ± 2.16 nm, was observed when DSAs were measured in RPMI and DMEM growth media, respectively (Figure 1B). The polydispersity index values in the range of 0.12−0.32 demonstrate that the generated self-assembly nanoparticles are uniformly dispersed with narrow size variation. The surface charge measurements of DSAs were found to be −15.1 ± 0.4, −15.5 ± 0.4, and −14.1 ± 0.3 mV in water (PBS), RPMI, and DMEM culture media, respectively (Figure 1C). The negative charge indicates stable formulation and shows no aggregation. Further, the TEM images of DSAs revealed its spherical morphology with the average particle size of 65.47 ± 5.38 nm (Figure 1D). The variation between DLS and TEM results in particle size was due to hydrated versus dehydrated form of DSAs. This size range of nanoparticles are widely used for preclinical and clinical studies and FDA-approved therapeutic applications which suggest that DSAs can be chosen for drug delivery applications.

Further, the formation of DSAs was affirmed through the availability of functional groups by FT-IR analysis. FT-IR spectra show the presence of various functional groups related absorption peaks for tannic acid and docetaxel (Figure 1E). The FT-IR spectrum of DSAs revealed that similar absorption bands that were present in the TA and Dtxl groups, manifesting the DSAs were constructed by these two self-assembly/complex formulations (Figure 1E). Among many, the distinct absorption band, 1700−1600 cm^{-1}, was associated with C−O stretching vibrations, while 1600−1500 cm^{-1} was due to NH bending with C−N stretching vibrations. From readings of TA and DSAs, we observed that the overlapping patterns of characteristic peaks at 1350−1320 cm^{-1} was associated with O−H stretching vibration of TA and Dtxl, 1180−1150 cm^{-1} annotating the presence of C−N stretching of Dtxl/DSAs. The molecular interactions among docetaxel and tannic acid in DSAs might be due to the occurrence of hydrogen bonding between ester groups of Dtxl and the phenolic groups of tannic acid. This suggests that there is no existing covalent bond formation. The XRD analysis displayed sharp crystalline peaks at 10° and 20° while DSAs exhibited a broader peak at 15° and 25° which was similar to the lyophilized tannic acid pattern, annotating its amorphous nature (Figure 1F). This indicates that docetaxel is deeply intercalated within tannic acid layers. Further, the thermogravimetric analysis of the DSAs exhibited similar degradation patterns to that of tannic acid due its encapsulated shell around the Dtxl cores (Figure 1G). Thermograms of DSAs apparently showed major weight loss

between 230 and 340 °C due to disruption among both inter- and intramolecular bonding of the constituent molecules. Overall, these results distinctly revealed the presence of tannic acid and docetaxel in DSAs formulation.

DSAs Exhibit Hemocompatibility.

It is necessary to prove the safety and reliability of new formulations using adequate *in vitro* hemocompatibility analyses for its successful implementation in *in vivo* studies and clinical translation.[51] There was negligible hemolysis of the RBCs after DSAs incubation ranging in concentration from 5 to 100 μg (equivalent to a Dtxl concentration range of 6.2−120 μmol/L). About 7.76% of hemolysis activity was noticed at the higher concentration of DSAs (100 μg) (Dtxl concentration 120 μmol/L), whereas docetaxel did not exhibit hemolytic activity until 5−20 μg (similar as DSAs) but 50 and 100 μg concentrations lead to 10.86% and 19.56% hemolysis. Tannic acid which was used to generate DSAs also did not show toxicity (Figure S1). These results were further evident from morphology analysis of RBCs (Figure 1H). Both TA and DSAs did not influence membrane integrity or morphology similar to the negative control (PBS). There was a drastic change in RBC shape with Dtxl exposure (Figure 1H). Altogether, these results specified that DSAs a displayed negligible amount of hemolytic activity and can be subsequently chosen for *in vivo* studies. These results also indicated that DSAs formulation is hemocompatible in comparison to docetaxel, indicating that DSAs are safe and can be subsequently chosen for *in vivo* studies.

In Vitro Cellular Uptake and Fate of DSAs.

To assess DSAs facilitate docetaxel uptake of tumor cells *in vitro*, a cellular uptake study was performed in prostate cancer cells. The results were evaluated looking at the extent of uptake by confocal and flow cytometry methods. Coumarin 6 in DSAs was used assist in tracking the nanoparticles in these assays. Flow cytometry analysis revealed that there was a consistent increase in mean fluorescence intensity (MFI) values with increasing DSAs concentration. This data indicates uptake of DSAs is a dose dependent process. DSAs showed superior internalization in C4–2 cells. The order of uptake phenomenon was noticed as C4–2 > PC-3 ≥ DU145 (Figure 2A–B). DSAs exhibited by visual evidence a cytoplasmic accumulation in prostate cancer cells after 3 h of incubation. In cellular fate analysis a 3 h incubation of DSAs demonstrated a distinct endosomal escape pattern in PC-3 cells. There was a yellow color fluorescence observed due to colocalization of DSAs (green) with early endosomal (red) marker (Figure 2C). This behavior is significantly less with late endosomal marker (Figure 2C). Such a colocalization pattern was completely missing with just lysosomes. This suggests that DSAs can evidently escape the endosome during the late endosome to lysosome fusion transition of the endocytic process.

To confirm the intracellular accumulation, native drug solution and DSAs were supplemented on PC-3 cells for 1, 2, and 6 h, and Dtxl was quantified utilizing LC-MS/MS. The calibration of a standard curve with an R^2 value of 0.99475 was developed and used for this quantification (Figure S2). Native drug solution could achieve a maximum of 43.94 ± 0.99% in 6 h, in contrast to Dtxl that demonstrates a maximum of 79.15 ± 6.61% (Figure 2D). Dtxl internalization was saturated within 2 h, and no change in cellular accumulation was observed at 6 h when native Dtxl was employed. There was 1.8−2.2-fold increase found

in Dtxl concentration accumulation with DSAs, suggesting that the TA binder indeed helped to enhance the intracellular drug concentration. Such behavior of tannic acid was noticed before in paclitaxel delivery.[33]

DSAs Inhibit Proliferation, Clonogenicity and Induce Apoptosis.

DSAs confirmed superior delivery deport of Dtxl into prostate cancer cell lines. Next, we examined potential anticancer effects of the DSAs via proliferation and clonogenic formation assays on three prostate cancer (C4–2, DU145, and PC-3) cell lines. In proliferation assay, docetaxel treatments alone (2.5−40 nM) showed significant inhibition of proliferation of cells, while DSAs (at the same concentration of Dtxl, 2.5−40 nM) demonstrated a substantially greater proliferation inhibition. For example, at 10 nM Dtxl, the percent proliferation remained at ~56%, 64%, and 66% in C4–2, DU145, and PC-3 cells. The percent proliferation of DSAs at the same was prominently reduced to ~44%, 47%, and 47%, respectively (Figure 3A). Overall, the cell proliferation results clearly deduced the enhanced efficacy of DSAs over Dtxl treatments. The superior clonogenic inhibitory activity of DSAs was evaluated by colony formation assay. Dtxl (2.5 and 5 nM) treatments exhibited reduction in the colonies while DSAs (equivalent to Dtxl 2.5 and 5 nM) showed a greater reduction in the number of colonies (Figure 3B–C). This data indicates that DSAs possess superior effects over Dtxl in inhibiting growth/proliferation of prostate cancer cells.

To evaluate the potential of DSAs as chemotherapy agents for prostate cancer, pro-apoptotic, apoptotic, and pro-survival proteins were examined using immunoblot analysis. As shown in Figure 3D, the decreased expression of Bcl-2 and Bcl-xL was observed with DSAs treatment, whereas enhanced expression was observed for pro-apoptotic and apoptosis-associated proteins (Bax and Cleaved PARP). These results were further confirmed through microarray studies, and the respective heat maps were presented (Figure 3E).

Microarray data analyzed through iPathwayGuide analysis indicated that DSAs interfere with cellular senescence in prostate cancer cells. To further validate our finding, we curated the expression fold of senescence signaling proteins and its biomarkers like TGFβR1, RB1(Rb), and CDKN1A (p21) in prostate cancer patients specifically using the *ONCOMINE* database.[42] Interestingly, we observed high expression of TGFβR1,[52,53] RB1(Rb),[54,55] and CDKN1A (p21)[52,56] within human prostate cancer samples in multiple data sets (Figure 4). The androgen deprivation status of the curated patient samples was provided in Supporting Information (Table S1). Further, to affirm these mechanistic results, we performed the protein profiling results in C4-2 and PC-3 cells treated with TA, Dtxl, and DSAs for 24 h (Figure 5).

DSAs Suppress Cell Senescence in Prostate Cancer Cells.

The senescence characteristic of prostate cancer cells can be attributed to a large and flattened morphology. Senescence-activated β-galactosidase (SA-β-gal) activity confirms the inherent senescence characteristics of cells (Figure 5A). In contrast, there was a high percentage of SA-β-galpositive cells that were observed during Dtxl treatments, denoting their negligible effects on senescence. DSAs treatment explicitly inhibited and lowered the cell percentage with SA-β-gal-positive staining. To ratify the senescence inhibition by

DSAs, the microarray studies were performed and analyzed through heat mapping and iPathwayGuide methods. The results demonstrated the antisenescence role of DSAs and their molecular specificity in inactivation of SASP related TGF-β signaling (Figure 5B), and other gene regulatory effects of DSAs were demonstrated using iPathwayGuide analysis (Figure S3A–E). The analysis of iPathwayGuide studies further disclosed that SASP signaling stands as one of the top signaling pathways that was markedly affected during the DSAs treatment in PC-3 cells (Figure S3C). Immunoblot analysis results evidently demonstrated that DSAs specifically target SASP-related signaling molecules by inhibiting TGFβR1, p21, and FOXO1 and restoring p-RB[57] in both cell lines, compared to control cells (Figure 5C). Conversely, there was no prominent effect on the expression of these proteins during Dtxl treatments. The gene regulatory effects of DSAs on SASP associated proteins was also confirmed through heat maps (Figure 5D). Altogether, these observations reveal the specific inhibitory effects of DSAs toward senescence signaling in prostate cancer cells.

Biodistribution and Tumor Targeting Potential of DSAs.

Nanoparticles are often cleared by various excretion processes.[58] For effective translation of a therapeutic nanoparticle formulation, it is required to circulate in the bloodstream long enough to allow tumor accumulation. To assess the track of biodistribution of DSAs, ICG dye and ICG-DSAs were injected by intraperitoneal administration into PC-3 tumor-bearing nude mice. A quantitative NIR fluorescence intensity evaluation of dye distribution in various organs of mice and tumor regions at different time-points. Both 3 and 6 h time points after injection, ICG dye showed diffused fluorescence intensity throughout the animal compared to ICG-DSAs. This confirms that ICG-DSAs enhanced blood circulation and thus had a higher level of presence in mice. After 48 h, ICG dye was eliminated from mice without reaching tumor site(s) (Figure 6A), whereas ICG-DSAs showed less clearance with accumulation capacity at the tumors. At 72 h, all ICG-DSAs reached and accumulated in tumors. This pattern of accumulation suggests that ICG-DSAs may not only enhance the circulation but improve tumor directed delivery of therapeutics. It is considered that the EPR effect is responsible for tumor accumulation of DSAs. *Ex vivo* fluorescence evaluation of dissected organs (heart, liver, spleen, lung, and kidney) and tumor tissue(s) at 72 h postinjection further confirmed the tumor-specific accumulation of DSAs (Figure 6B). Further, we represented the ROI values graphically in Figure 6C. Altogether, the DSAs effectively targeted tumors 72 h postinjection in all mice. These results demonstrate that DSAs can be deported to the tumor sites and thus the DSAs formulation is suitable for docetaxel delivery to prostate cancer cells.

DSAs Induce Regression of PC-3 Tumor Xenografts.

The above results indicated tumor specific accumulation of nanoparticles. Additionally, tannic acid which is used as a nanocarrier matrix can bind/target various oncogenic proteins (which abundantly exist) on tumor cells;[21] thus DSAs may strongly binds to tumors cells and release therapeutics for improved therapeutic outcomes. Therefore, we assessed the therapeutic efficacy of DSAs using male mice (nu/nu) bearing PC-3 subcutaneous xenografts twice, but the data is shown from one of the studies. After tumors reached sizes of ~100 mm^3, mice were randomized in four groups. The dose of Dtxl 30 mg/kg (maximal

tolerated dose (MTD)) was administered through intraperitoneal injections for therapeutic evaluation.[38] The four groups of randomized mice were treated with (i) vehicle control (PBS), (ii) TA (38 mg/kg), (iii) Dtxl (30 mg/kg), and (iv) DSAs (Dtxl equivalent, 30 mg/kg). The tumor size and body weight were then monitored for 4 weeks. Control group (PBS) mice demonstrated continued tumor growth which reached 814 ± 75 mm^3. TA treatment exhibited some effect on tumor growth (Figure 7A–C), but it was not significant. The tumors in the Dtxl group grew slowly and reached 287 ± 51 mm^3. The growth in the DSA group was further reduced to 191 ± 28 mm^3. Among all groups, tumorgrowth delay was significantly enhanced with DSAs (Figure 7A). At the end of study, mice were sacrificed, and the tumors were collected and weighed (Figure 7D). The mean weight of the tumors in the DSAs group was the smallest among the other groups. The immuno-histochemistry revealed activation of apoptotic protein (Cl. PARP) and decrease in pro-survival (Bcl-xL), drug resistance (MDR1), and proliferation (PCNA) proteins by DSAs treatments (Figure 7E). Altogether, these results disclose the enhanced apoptotic and tumor regressing ability of DSAs.

DSAs Inhibit Senescence in PC-3 Tumors.

To confirm the *in vivo* antisenescence role of DSAs we performed β-galactosidase staining among excised tumor tissues. Previous reports state that elevated expression of tumorigenic genes induces senescence in cancer tissues, and the term oncogene-induced senescence (OIS) was coined for this.[59,60] From *ex vivo* β-galactosidase staining, we observed a greater number of senescence associated β-galactosidase (SA-β-gal) + ve cells in tumors treated with PBS (Ctrl) and Dtxl resulting in prominent green stain in the tissues. Control PC-3 cells *in vitro* (Figure 5A) exhibited β-galactosidase staining supporting the control tumors are positive for senescence marker. This high degree of staining is partly due to tumor cells which may have undergone growth arrest conditions because of having no growth medium and factors. We believe that OIS might have played a pivotal role in staining the untreated tumor excised tissues. Contrastingly, there was negligible amount stain observed in the DSA treated tumors indicating the smaller number of SA-β-gal + ve cells (Figure 8A). Further, the relative absorbance of the tissue incubated staining solution was measured (Figure 8B). From the results, it was evident that relative absorbance of staining solution that was incubated with DSA treated tumors was lower than all other treatment groups, denoting the antisenescence ability of DSAs.

DSAs Blockade TGF-β Mediated Senescence Signaling and Activate Apoptotic Events in PC-3 Tumor Xenografts.

To validate the antisenescence ability of DSAs and reduction of tumor growth, we sectioned PC-3 tumor mouse xenograft tissues and examined them for TGF-β mediated SASP expression using IHC. As shown in Figure 8C, DSAs treatment resulted selective deregulated TGFβR1 expression and its downstream target p21 was reduced compared to control, TA, and Dtxl treatment groups. In contrast, the p-Rb was induced effectively upon DSAs treatment; this strongly confirms that DSAs prevent or reverse the drug-induced cellular senescence. The antiproliferative ability of DSAs was demonstrated by the descending expression patterns of PCNA (a proliferation marker) and Bcl-xL (pro-survival protein). In addition, the expression of MDR1 (chemo-resistance indicator) in the DSAs

group was found to be the lowest among all groups, this indicates that DSAs exhibit chemo-sensitization characteristics. Consistent with the *in vitro* superior apoptotic potential of the formulation, there was profound expression of cleaved PARP during DSAs treatments, observed due to its enhanced antitumor effects. Altogether, these results suggest that DSA treatment diminishes the senescence signaling, enhances chemo-sensitization, and subsequently activated the apoptotic signaling events in PC-3 tumors.

DSAs Exhibited *in vivo* Biophysiological and Biocompatible Attributes.

To identify hemocompatibility and safety of DSAs compared to docetaxel drug solution, morphology and histological studies were performed on erythrocytes and other major organs of mice. The morphology of erythrocytes treated with DSAs were intact and resembled the control (PBS) and TA treatment groups. There were prominent morphological changes observed with the Dtxl treatments group (Figure 9A). The results clearly indicate the nontoxicity of DSAs to RBC membranes of mice, which coincides with results of the *ex vivo* hemocompatibility as described in the earlier section.

Furthermore, ALT, AST, ALP, TBili, Alb, Create, BUN, Ca, and Glu in mice treated with DSAs fell within the normal ranges, suggesting no significant liver and renal toxicity (Table 1). In addition, there was no evidence of functional toxicity of the heart, liver, kidney, or spleen. No obvious damage was observed in H&E staining of the major organs in the DSAs treated group (Figure 9B). Collectively, these results are indicative that our nanoformulation at this dose is tolerable and safe *in vivo*. These results demonstrated that when compared with free Dtxl drug solution, DSAs formulation exhibited hemocompatibility, biocompatibility, shelf stability, and the least systemic toxicity.

DISCUSSION

Docetaxel has a long clinical track record in cancer treatment, including in prostate cancer therapies.[61] Docetaxel nanoparticle formulations (especially liposomal-based formulations) have emerged as therapeutic nanoplatforms for nanomedicine application.[62] Although, nanoparticle formulations minimize systemic toxicity and improve reservoirs of the drug at the tumors, they are still unable to tackle drug resistance and the development of the senescence phenomenon. Therefore, the aim of the present study was to examine the superior anticancer activity of docetaxel at the tumor site by using a unique docetaxel−tannic acid self-assembly formulation which can inhibit drug resistance and eliminate senescent cells. Tannic acid employed in the generation of DSAs not only offers the formation of assemblies with miscibility toward an aqueous environment, biocompatibility, and stability to the assembly formulation, but it exhibited inherent anticancer, tumor preventive, and tumor targeting characteristics.[24,25] Thus, it was anticipated the DSAs formulation can provide a unique opportunity to accumulate at the tumor sites and modulate the drug resistance and senescence profiles of tumor cells and thereby maximize the anticancer performance.

Therapeutic nanoparticles or nanomedicine of various small and biomacromolecules are widely investigated for improved therapeutic benefit over conventional agents in cancer treatments. So far over 75 nanomedicine treatments are in clinical practice for various

indications. This is primarily due to improved bioavailability, biodegradability, low systemic toxicity, and targeted and controlled drug delivery. According to our knowledge, there is no study aimed at targeting senescent cells in prostate cancer therapy using nanoparticle-based treatment. We opted tannic acid to produce docetaxel self-assemblies due to hydrogen bonding. The characterization results of DSAs, such as particles size, surface charge, spectroscopy, crystallinity, and thermal properties (Figure 1) discernibly attributed indicates an optimized size of the nanoparticle and requisite composition for cancer therapy. The negligible percent of hemolysis ascribed to the nanoformulation's hemocompatibility and thus can be chosen for drug delivery applications.[51] In addition, the cellular uptake results disclosed there was a superior cellular internalization and late endosomal escape mechanism of DSAs (Figure 2A–C).

Our study indicated DSAs efficiently delivered docetaxel (79.15 ± 6.61%) compared to free docetaxel drug in solution (43.94 ± 0.99%) in cancer cells (Figure 2D). This explains the mechanism of enhanced delivery of drug(s) which can offer superior anticancer activity over native drug treatments. This was further confirmed from superior anticancer potential of DSAs in various functional assays (Figure 3A–C). Further, *in vitro* results affirmed that the effects of DSAs at protein level (Figure 3D–E): the activation of apoptotic signaling (by downregulating the expression of antiapoptotic proteins, Bcl-2 and Bcl-xL) and simultaneously induction of the intracellular Bax and Cleaved PARP proteins. Gene microarray analysis of cells treated with DSAs profoundly activated the apoptotic genes thus enabling the superior antitumor activity of the formulation against prostate cancer. Hence, we believe that presence of TA in the formulation might not only enable the formation of DSAs along with Dtxl but also aggrandize the therapeutic behavior of Dtxl.

Cellular senescence is a mechanism program of cell-cycle arrest, in which cells do not proliferate but remain metabolically active and influence biological processes. At the cellular level, signaling players, like growth factors, extracellular matrix components, and cytokines are referred to as SASP.[63] Clearance of senescent cells from the tumors and its microenvironment has been known to have clinical benefit.[11,12] On the other side, accumulation of senescent cells could offer a substantial repository for future metastasis and cancer relapse. Thus, targeting senescence associated signaling in these cells using SASP inhibitors was established, and its clinical outcome is quite promising.[64] However, SASP inhibitors exhibit toxicological and inflammatory issues.[65] In order to subdue these clinical complications, there is a need for strategic therapy that specifically targets senescence signaling in cancer cells. In this note, we designed DSAs, a novel nanoformulation that selectively inhibits senescence signaling in prostate cancer. In this study, it was proven through the microarray and iPathwayGuide analysis that DSAs influence targeted senescence signaling besides apoptotic signaling among the top pathways. To date very few studies have been reported on nanoparticles targeting senescent cells.[14,66,67] Our strategic treatment approach by DSAs modulated senescence signaling through inhibition of TGFβR1/FOXO/p21 signaling axis (Figure 10). The immunoblotting results discerned the targeted inhibition of senescence related TGFβR1, FOXO1, and p21 proteins during DSAs exposure, while there was an increase in p-Rb proteins levels (Figure 5C). Further, the antisenescence inhibitory role of DSAs was confirmed through β-galactosidase staining assay in both *in vitro* and *ex vivo* studies. It is anticipated that docetaxel−tannic acid

assemblies and tannic acid layers on self-assemblies are capable of maintaining structural and stability of formulation. Tannic acid layers/units in the DSAs can presumably offer the following: (i) stability in blood circulation, (ii) minimized opsonization, and (iii) targeted delivery to tumors. Also, DSAs exhibited superior tumor accumulation in the nanoparticle targeting *in vivo*. This tumor targeting assessment of DSAs further warrants its clinical implications.[68] The translation to a preclinical level, however, requires a complete biodistribution study. Conventional nanoparticle drug formulations are often cleared from the body via the reticuloendothelial system, which ends in the liver and spleen.[58] The DSAs proved to have superior bioavailability while a significant portion reached to the tumor sites. Thus, the tumor targeting potential of DSAs favored significant tumor growth inhibition during nanoformulation treatments.

This study advises that this DSA formulation can potentially eliminate senescence cells by inhibiting TGFβR1, a member of the regulatory proteins that is specific and responsible for cell survival.[69] Recent studies show that senescent cells present therapeutic resistance in cancer and their elimination offers better therapeutic benefits.[70] It is apparent that DSAs treatment showed a tumor-regressing pattern compared to free docetaxel administered mice implanted PC-3 tumor cell xenografts. It is important to note that TA alone had no effect on tumor regression. The primary reasons (in addition to the conventional therapeutic activity of docetaxel) for such tumor regression activity may be the elimination of senescent tumor cells by inhibition of TGFβR1 and p21 senescence associated proteins and induction of p-Rb levels. Mice treated with DSAs formulation showed barely any senescence associated β-galactosidase activity (less blue stain intensity) indicating the elimination or absence of senescence. A significant senescence associated β-galactosidase activity can be seen in all other treatment groups. In addition, our observations further reinforce that docetaxel entrapped in tannic acid efficiently delivered Dtxl inducing efficient delivery cell death through inhibition of Bcl-xL and enhancement of the intracellular accumulation of cleaved PARP in tumor cells. The DSAs formulation also showed increased inhibition of cell proliferation and survival proteins like PCNA and MDR1 proteins over docetaxel treatment. This indicates an enhanced chemosensitization and apoptotic potential of DSAs along with inhibition of senescence.

Nanomedicines are often constructed to achieve tumor specific targeting, however, before they reach tumors, and a huge population of nanoparticles are in direct contact with blood cells. Therefore, hemocompatibility is one other standard indicative of clinical applicability. A safe nanomedicine while in circulation needs to have limited effect on erythrocytes to safely deposit the therapy in the tumor. Thus, hemocompatibility is useful as an initial screening assay to confirm the nontoxic interaction of nanomedicine with blood components. Our study demonstrated the *in vitro* and *in vivo* hemocompatibility of DSAs in whole human and mice blood, respectively. Additionally, a lack of inflammatory responses and normal ranges of serum proteins were observed with DSAs treatments, which indicates its potential therapeutic implications.

The moderate increase in the antitumor efficacy of DSAs over docetaxel might be due to passive targeting of the nanoformulation (Figures 6–7). The greater accumulation of DSAs formulation indicates its capability to reach tumors due to hypervascularity, leakiness, and

absence of lymphatic drainage. The docetaxel drug delivered through DSAs has shown greater therapeutic benefits. For such effects, there may be many reasons. Among those, one of them is circumvention of cellular senescence. The inhibition role of DSAs on senescence further needs to be validated in orthotopic mouse model of prostate cancer and the transgenic adenocarcinoma of the mouse prostate (TRAMP) models. Further, there is a need to compare mitotic catastrophe and related signaling by the free drug and the DSAs to this study.

All these observations reinforce the concept that DSAs are a useful nanoplatform to deliver docetaxel or any other anticancer molecules to tumor cells to achieve improved therapeutic benefits while eliminating or minimizing senescent and drug resistant tumor cells. Such nanomedicine enhances therapeutic effects and minimizes the dose of therapeutic agent required for effective therapy and number of doses required for therapy.

CONCLUSION

This study develops and narrates a novel DSAs formulation that specifically targets senescence signaling and offers chemosensitization in prostate cancer. The prepared DSAs formulation exhibited a monodispersed and biocompatible formulation with optimal size and surface charges that facilitates effective delivery of Dtxl to prostate cancer cells. The DSAs formulation displayed profound therapeutic activity against prostate cancer by inhibiting TGFβR1/FOXO1/p21 mediated senescence and inducing apoptosis in prostate cancer cells and tumor xenografts. Further, preclinical and clinical studies are warranted to implement this formulation for treating drug induced senescence prostate tumors.

Supplementary Material

Refer to Web version on PubMed Central for supplementary material.

ACKNOWLEDGMENTS

Molecular Resource Center (fluorescence measurements, micro-array, and iPathwayGuide analysis), Office of Research (editorial assistance), Shared Instrument and Flow cytometry Facility (FT-IR and flow cytometry) of the University of Tennessee Health Science Center and Department of Chemistry (University of Nebraska Medical Center, Lincoln, NE) (TGA analysis) help in acquisition of data are highly acknowledged. The authors acknowledge Mr. Kyle Doxtater for his help in editing this manuscript and Mr. Mehdi Chaib for his suggestions.

Funding

This work was supported by the National Institute of Health/National Cancer Institute's funding K22 CA174841 and Start up from UTHSC to M.M.Y. The studies were also grateful for partial support from the National Institute of Health grants R01 CA210192, R01 CA206069, and R01 CA204552 and Start up from UTHSC to S.C.C.

ABBREVIATIONS

DSAs	docetaxel self-assemblies
Dtxl	docetaxel
MDR	multidrug resistance
SA-β-gal	β-galactosidase

NP	nanoparticle
SASP	senescence associated secretory phenotype
TA	tannic acid
DLS	dynamic light scattering
TEM	transmission electron microscopy
FT-IR	Fourier transform infrared spectroscopy
XRD	X-ray diffraction
TGA	thermogravimetric analysis
LC-MS/MS	liquid chromatography-tandem mass spectrometry
Ptxl	paclitaxel
AAALAC	Association for Assessment and Accreditation of Laboratory Animal Care
ICG	Indocyanine green
CCD	coupled device camera
AST	aspartate aminotransferase
ALT	alanine aminotransferase
ALP	alkaline phosphatase
TP	total protein
Tbili	total bilirubin
Alb	albumin
Create	creatinine
BUN	blood urea nitrogen
Ca	calcium
Glu	glucose
IHC	immuno-histo-chemical studies

REFERENCES

(1). Siegel RL; Miller KD; Jemal A. Cancer Statistics, 2019. Ca-Cancer J. Clin 2019, 69 (1), 7–34. [PubMed: 30620402]

(2). Quinn DI; Sandler HM; Horvath LG; Goldkorn A; Eastham JA The Evolution of Chemotherapy for the Treatment of Prostate Cancer. Ann. Oncol 2017, 28 (11), 2658–2669. [PubMed: 29045523]

(3). Becker DJ; Iyengar AD; Punekar SR; Ng J; Zaman A; Loeb S; Becker KD; Makarov D. Treatment of Metastatic Castration-resistant Prostate Cancer With Abiraterone and Enzalutamide Despite PSA Progression. Anticancer Res. 2019, 39 (5), 2467–2473. [PubMed: 31092441]

(4). Hanninen M; Venner P; North S. A Rapid PSA Half-Life Following Docetaxel Chemotherapy is Associated With Improved Survival in Hormone Refractory Prostate Cancer. Can. Urol Assoc J 2009, 3 (5), 369–374. [PubMed: 19829727]

(5). Tassinari D; Cherubini C; Roudnas B; Tamburini E; Drudi F; Bianchi E; Fantini M; Montanari F; Sartori S. Treatment of Metastatic, Castration-resistant, Docetaxel-resistant Prostate Cancer: A Systematic Review of Literature With a Network Meta-analysis of Randomized Clinical Trials. Rev. Recent Clin. Trials 2018, 13 (3), 226–237. [PubMed: 29623850]

(6). Orr GA; Verdier-Pinard P; McDaid H; Horwitz SB Mechanisms of Taxol Resistance Related to Microtubules. Oncogene 2003, 22 (47), 7280–7295. [PubMed: 14576838]

(7). Luqmani Y. Mechanisms of Drug Resistance in Cancer Chemotherapy. Medical Principles and Practice 2005, 14 (1), 35−48.

(8). Gordon RR; Nelson PS Cellular Senescence and Cancer Chemotherapy Resistance. Drug Resist. Updates 2012, 15 (1−2), 123–131.

(9). Ewald JA; Desotelle JA; Wilding G; Jarrard DF Therapy-Induced Senescence in Cancer. J. Natl. Cancer Inst 2010, 102 (20), 1536–1546. [PubMed: 20858887]

(10). Zhang Y; Alexander PB; Wang XF TGF-beta Family Signaling in the Control of Cell Proliferation and Survival. Cold Spring Harbor Perspect. Biol 2017, 9 (4), a022145.

(11). Xue W; Zender L; Miething C; Dickins RA; Hernando E; Krizhanovsky V; Cordon-Cardo C; Lowe SW Senescence and Tumour Clearance is Triggered by p53 Restoration in Murine Liver Carcinomas. Nature 2007, 445 (7128), 656–660. [PubMed: 17251933]

(12). Dimri GP; Lee X; Basile G; Acosta M; Scott G; Roskelley C; Medrano EE; Linskens M; Rubelj I; Pereira-Smith O. A Biomarker that Identifies Senescent Human Cells in Culture and in Aging Skin In vivo. Proc. Natl. Acad. Sci. U. S. A 1995, 92 (20), 9363–9367. [PubMed: 7568133]

(13). O'Neill AJ; Prencipe M; Dowling C; Fan Y; Mulrane L; Gallagher WM; O'Connor D; O'Connor R; Devery A; Corcoran C; Rani S; O'Driscoll L; Fitzpatrick JM; Watson RW Characterisation and Manipulation of Docetaxel Resistant Prostate Cancer Cell lines. Mol. Cancer 2011, 10, 126. [PubMed: 21982118]

(14). Muñoz-Espín D; Rovira M; Galiana I; Giménez C; Lozano-Torres B; Paez-Ribes M; Llanos S; Chaib S; Muñoz-Martín M; Ucero AC; Garaulet G; Mulero F; Dann SG; VanArsdale T; Shields DJ; Bernardos A; Murguía JR; Martínez-Máñez R; Serrano M. A Versatile Drug Delivery System Targeting Senescent Cells. EMBO Molecular Medicine 2018, 10, No. e9355.

(15). Subbiah R; Veerapandian M; Yun KS Nanoparticles: Functionalization and Multifunctional Applications in Biomedical Sciences. Curr. Med. Chem 2010, 17 (36), 4559–4577. [PubMed: 21062250]

(16). Tran S; DeGiovanni PJ; Piel B; Rai P. Cancer Nanomedicine: A Review of Recent Success in Drug Delivery. Clin Transl Med. 2017, 6 (1), 44. [PubMed: 29230567]

(17). Hoshyar N; Gray S; Han H; Bao G. The Effect of Nanoparticle Size on In vivo Pharmacokinetics and Cellular Interaction. Nanomedicine (London, U. K.) 2016, 11 (6), 673–692.

(18). Ciurana J; Rodriguez CA Trends in Nanomaterials and Processing for Drug Delivery of Polyphenols in the Treatment of Cancer and Other Therapies. Curr. Drug Targets 2016, 18 (2), 135–146.

(19). Davatgaran-Taghipour Y; Masoomzadeh S; Farzaei MH; Bahramsoltani R; Karimi-Soureh Z; Rahimi R; Abdollahi M. Polyphenol Nanoformulations For Cancer Therapy: Experimental Evidence and Clinical Perspective. Int. J. Nanomed 2017, 12, 2689–2702.

(20). Karakurt S; Adali O. Tannic Acid Inhibits Proliferation, Migration, Invasion of Prostate Cancer and Modulates Drug Metabolizing and Antioxidant Enzymes. Anti-Cancer Agents Med. Chem 2016, 16 (6), 781–789.

(21). Darvin P; Joung YH; Kang DY; Sp N; Byun HJ; Hwang TS; Sasidharakurup H; Lee CH; Cho KH; Park KD; Lee HK; Yang YM Tannic acid Inhibits EGFR/STAT1/3 and Enhances p38/STAT1 Signalling Axis in Breast Cancer Cells. Journal of Cellular and Molecular Medicine 2017, 21 (4), 720–734. [PubMed: 27862996]

(22). Naus PJ; Henson R; Bleeker G; Wehbe H; Meng F; Patel T. Tannic acid Synergizes the Cytotoxicity of Chemotherapeutic Drugs in Human Cholangiocarcinoma by Modulating Drug Efflux Pathways. J. Hepatol 2007, 46 (2), 222–229. [PubMed: 17069924]

(23). Darvin P; Baeg SJ; Joung YH; Sp N; Kang DY; Byun HJ; Park JU; Yang YM Tannic acid Inhibits the Jak2/STAT3 Pathway and Induces G1/S Arrest and Mitochondrial Apoptosis in YD-38 Gingival Cancer Cells. Int. J. Oncol 2015, 47 (3), 1111–1120. [PubMed: 26202061]

(24). Nagesh PKB; Hatami E; Chowdhury P; Kashyap VK; Khan S; Hafeez BB; Chauhan SC; Jaggi M; Yallapu MM Tannic Acid Induces Endoplasmic Reticulum Stress-Mediated Apoptosis in Prostate Cancer. Cancers 2018, 10 (3), 68.

(25). Hatami E; Nagesh PKB; Chowdhury P; Kashyap VK; Khan S; Hafeez B; Jaggi M; Chauhan SC; Yallapu MM Abstract LB-400: Tannic acid Induces Prostate Cancer Cell Death via Unfolded Protein Response (UPR) and Modulation of CHOP. Cancer Res. 2018, 78 (13Supplement), LB-400−LB-400.

(26). Autio KA; Dreicer R; Anderson J; Garcia JA; Alva A; Hart LL; Milowsky MI; Posadas EM; Ryan CJ; Graf RP; Dittamore R; Schreiber NA; Summa JM; Youssoufian H; Morris MJ; Scher HI Safety and Efficacy of BIND-014, a Docetaxel Nanoparticle Targeting Prostate-Specific Membrane Antigen for Patients With Metastatic Castration-Resistant Prostate Cancer: A Phase 2 Clinical Trial. JAMA Oncol 2018, 4 (10), 1344–1351. [PubMed: 29978216]

(27). Dubey S; Thomas A; Samanta MK Development of Docetaxel-PLGA-Nanoparticles and In Vitro anti-tumor activity in PC3 cells Targeted to Prostate Tumor. Int. J. Sci. Eng. Res 2016, 7, 671–678.

(28). Hwang C. Overcoming Docetaxel Resistance in Prostate Cancer: A Perspective Review. Ther. Adv. Med. Oncol 2012, 4 (6), 329–340. [PubMed: 23118808]

(29). Galletti E; Magnani M; Renzulli ML; Botta M. Paclitaxel And Docetaxel Resistance: Molecular Mechanisms and Development of New Generation Taxanes. ChemMedChem 2007, 2 (7), 920–942. [PubMed: 17530726]

(30). Seruga B; Ocana A; Tannock IF Drug Resistance in Metastatic Castration-Resistant Prostate Cancer. Nat. Rev. Clin. Oncol 2011, 8, 12. [PubMed: 20859283]

(31). Toso A; Revandkar A; Di Mitri D; Guccini I; Proietti M; Sarti M; Pinton S; Zhang J; Kalathur M; Civenni G; Jarrossay D; Montani E; Marini C; Garcia-Escudero R; Scanziani E; Grassi F; Pandolfi Pier P.; Catapano Carlo V.; Alimonti A. Enhancing Chemotherapy Efficacy in Pten-Deficient Prostate Tumors by Activating the Senescence-Associated Antitumor Immunity. Cell Rep. 2014, 9 (1), 75–89. [PubMed: 25263564]

(32). Fan H; Wang L; Feng X; Bu Y; Wu D; Jin Z. Supramolecular Hydrogel Formation Based on Tannic Acid. Macromolecules 2017, 50 (2), 666–676.

(33). Chowdhury P; Nagesh PKB; Hatami E; Wagh S; Dan N; Tripathi MK; Khan S; Hafeez BB; Meibohm B; Chauhan SC; Jaggi M; Yallapu MM Tannic acid-Inspired Paclitaxel Nanoparticles for Enhanced Anticancer Effects in Breast Cancer Cells. J. Colloid Interface Sci 2019, 535, 133–148. [PubMed: 30292104]

(34). Corona G; Elia C; Casetta B; Frustaci S; Toffoli G. High-throughput Plasma Docetaxel Quantification by Liquid Chromatography-Tandem Mass Spectrometry. Clin. Chim. Acta 2011, 412 (3−4), 358–64. [PubMed: 21078312]

(35). Karthik S; Prashanth Kumar BN; Gangopadhyay M; Mandal M; Singh NDP A Targeted, Image-Guided and Dually Locked Photoresponsive Drug Delivery System. J. Mater. Chem. B 2015, 3 (5), 728–732. [PubMed: 32262161]

(36). Boya VN; Lovett R; Setua S; Gandhi V; Nagesh PKB; Khan S; Jaggi M; Yallapu MM; Chauhan SC Probing Mucin interaction Behavior of Magnetic Nanoparticles. J. Colloid Interface Sci 2017, 488 (SupplementC), 258–268. [PubMed: 27837716]

(37). Nagesh PKB; Chowdhury P; Hatami E; Boya VKN; Kashyap VK; Khan S; Hafeez BB; Chauhan SC; Jaggi M; Yallapu MM miRNA-205 Nanoformulation Sensitizes Prostate Cancer Cells to Chemotherapy. Cancers 2018, 10 (9), 289.

(38). Nagesh PKB; Johnson NR; Boya VKN; Chowdhury P; Othman SF; Khalilzad-Sharghi V; Hafeez BB; Ganju A; Khan S; Behrman SW; Zafar N; Chauhan SC; Jaggi M; Yallapu MM PSMA

Targeted Docetaxel-Loaded Superparamagnetic Iron oxide Nanoparticles for Prostate Cancer. Colloids Surf., B 2016, 144, 8–20.

(39). Kumar BNP; Puvvada N; Rajput S; Sarkar S; Das SK; Emdad L; Sarkar D; Venkatesan P; Pal I; Dey G; Konar S; Brunt KR; Rao RR; Mazumdar A; Kundu SC; Pathak A; Fisher PB; Mandal M. Sequential Release of Drugs from Hollow Manganese Ferrite Nanocarriers for Breast Cancer Therapy. J. Mater. Chem. B 2015, 3 (1), 90–101. [PubMed: 32261929]

(40). Chowdhury P; Nagesh PKB; Khan S; Hafeez BB; Chauhan SC; Jaggi M; Yallapu MM Development of Polyvinylpyrrolidone/Paclitaxel Self-assemblies for Breast Cancer. Acta Pharm. Sin. B 2018, 8, 602–614. [PubMed: 30109184]

(41). Kalita H; Prashanth Kumar BN; Konar S; Tantubay S; Mahto M. Kr.; Mandal M; Pathak A. Sonochemically Synthesized Biocompatible Zirconium Phosphate Nanoparticles for pH Sensitive Drug Delivery Application. Mater. Sci. Eng., C 2016, 60, 84–91.

(42). Rhodes DR; Yu J; Shanker K; Deshpande N; Varambally R; Ghosh D; Barrette T; Pander A; Chinnaiyan AM ONCOMINE: A Cancer Microarray Database and Integrated Data-Mining Platform. Neoplasia 2004, 6 (1), 1–6. [PubMed: 15068665]

(43). Prashanth Kumar BN; Rajput S; Bharti R; Parida S; Mandal M. BI2536 − A PLK Inhibitor Augments Paclitaxel Efficacy in Suppressing Tamoxifen Induced Senescence and Resistance in Breast Cancer Cells. Biomed. Pharmacother 2015, 74, 124–132. [PubMed: 26349973]

(44). Hafeez BB; Ganju A; Sikander M; Kashyap VK; Hafeez ZB; Chauhan N; Malik S; Massey AE; Tripathi MK; Halaweish FT; Zafar N; Singh MM; Yallapu MM; Chauhan SC; Jaggi M. Ormeloxifene Suppresses Prostate Tumor Growth and Metastatic Phenotypes via Inhibition of Oncogenic β-catenin Signaling and EMT Progression. Mol. Cancer Ther 2017, 16 (10), 2267–2280. [PubMed: 28615299]

(45). Zheng M; Zhao P; Luo Z; Gong P; Zheng C; Zhang P; Yue C; Gao D; Ma Y; Cai L. Robust ICG Theranostic Nanoparticles for Folate Targeted Cancer Imaging and Highly Effective Photothermal Therapy. ACS Appl. Mater. Interfaces 2014, 6 (9), 6709–6716. [PubMed: 24697646]

(46). Zhuang J; Zhang J; Lwin ST; Edwards JR; Edwards CM; Mundy GR; Yang X. Osteoclasts in Multiple Myeloma are Derived from Gr-1+CD11b+Myeloid-Derived Suppressor Cells. PLoS One 2012, 7 (11), No. e48871.

(47). Li M; Xing S; Zhang H; Shang S; Li X; Ren B; Li G; Chang X; Li Y; Li W. A Matrix Metalloproteinase Inhibitor Enhances Anti-cytotoxic T lymphocyte antigen-4 Antibody Immunotherapy in Breast Cancer by Reprogramming the Tumor Microenvironment. Oncol. Rep 2016, 35 (3), 1329–1339. [PubMed: 26752000]

(48). Kumar BNP; Puvvada N; Rajput S; Sarkar S; Mahto MK; Yallapu MM; Pathak A; Emdad L; Das SK; Reis RL; Kundu SC; Fisher PB; Mandal M. Targeting of EGFR, VEGFR2, and Akt by Engineered Dual Drug Encapsulated Mesoporous Silica-Gold Nanoclusters Sensitizes Tamoxifen-Resistant Breast Cancer. Mol. Pharmaceutics 2018, 15 (7), 2698–2713.

(49). Kashyap VK; Wang Q; Setua S; Nagesh PKB; Chauhan N; Kumari S; Chowdhury P; Miller DD; Yallapu MM; Li W; Jaggi M; Hafeez BB; Chauhan SC Therapeutic Efficacy of a Novel BetaIII/BetaIV-tubulin Inhibitor (VERU-111) in Pancreatic Cancer. J. Exp. Clin. Cancer Res 2019, 38 (1), 29. [PubMed: 30674344]

(50). Luo J; Lai J; Zhang N; Liu Y; Liu R; Liu X. Tannic Acid Induced Self-Assembly of Three-Dimensional Graphene with Good Adsorption and Antibacterial Properties. ACS Sustainable Chem. Eng 2016, 4 (3), 1404–1413.

(51). Venkatesan P; Puvvada N; Dash R; Prashanth Kumar BN; Sarkar D; Azab B; Pathak A; Kundu SC; Fisher PB; Mandal M. The Potential of Celecoxib-Loaded Hydroxyapatite-Chitosan Nanocomposite for the Treatment of Colon Cancer. Biomaterials 2011, 32, 3794. [PubMed: 21392822]

(52). Magee JA; Araki T; Patil S; Ehrig T; True L; Humphrey PA; Catalona WJ; Watson MA; Milbrandt J. Expression Profiling Reveals Hepsin Overexpression in Prostate Cancer. Cancer Res. 2001, 61 (15), 5692–5696. [PubMed: 11479199]

(53). Arredouani MS; Lu B; Bhasin M; Eljanne M; Yue W; Mosquera J-M; Bubley GJ; Li V; Rubin MA; Libermann TA; Sanda MG Identification of the Transcription Factor Single-Minded

Homologue 2 as a Potential Biomarker and Immunotherapy Target in Prostate Cancer. Clin. Cancer Res. 2009, 15 (18), 5794–5802. [PubMed: 19737960]

(54). LaTulippe E; Satagopan J; Smith A; Scher H; Scardino P; Reuter V; Gerald WL Comprehensive Gene Expression Analysis of Prostate Cancer Reveals Distinct Transcriptional Programs Associated with Metastatic Disease. Cancer Res. 2002, 62 (15), 4499–4506. [PubMed: 12154061]

(55). Welsh JB; Sapinoso LM; Su AI; Kern SG; Wang-Rodriguez J; Moskaluk CA; Frierson HF; Hampton GM Analysis of Gene Expression Identifies Candidate Markers and Pharmacological Targets in Prostate Cancer. Cancer Res. 2001, 61 (16), 5974–5978. [PubMed: 11507037]

(56). Holzbeierlein J; Lal P; LaTulippe E; Smith A; Satagopan J; Zhang L; Ryan C; Smith S; Scher H; Scardino P; Reuter V; Gerald WL Gene expression analysis of human prostate carcinoma during hormonal therapy identifies androgen-responsive genes and mechanisms of therapy resistance. Am. J. Pathol 2004, 164 (1), 217–227. [PubMed: 14695335]

(57). Obreque-Slier E; Mateluna C; Pena-Neira A; Lopez-Solis R. Quantitative Determination of Interactions Between Tannic Acid and a Model Protein Using Diffusion and Precipitation Assays on Cellulose Membranes. J. Agric. Food Chem 2010, 58 (14), 8375–8379. [PubMed: 20583840]

(58). Alexis F; Pridgen E; Molnar LK; Farokhzad OC Factors Affecting the Clearance and Biodistribution of Polymeric Nanoparticles. Mol. Pharmaceutics 2008, 5 (4), 505–515.

(59). Collado M; Gil J; Efeyan A; Guerra C; Schuhmacher AJ; Barradas M; Benguria A; Zaballos A; Flores JM; Barbacid M; Beach D; Serrano M. Tumour biology: senescence in premalignant tumours. Nature 2005, 436 (7051), 642. [PubMed: 16079833]

(60). Senturk S; Mumcuoglu M; Gursoy-Yuzugullu O; Cingoz B; Akcali KC; Ozturk M. Transforming growth factor-beta induces senescence in hepatocellular carcinoma cells and inhibits tumor growth. Hepatology 2010, 52 (3), 966–74. [PubMed: 20583212]

(61). Puente J; Grande E; Medina A; Maroto P; Lainez N; Arranz JA Docetaxel in Prostate Cancer: A Familiar Face as the New Standard in a Hormone-Sensitive Setting. Ther Adv. Med. Oncol 2017, 9 (5), 307–318. [PubMed: 28529548]

(62). Zhang L; Zhang N. How Nanotechnology Can Enhance Docetaxel Therapy. Int. J. Nanomed 2013, 8, 2927–2941.

(63). Yang L; Fang J; Chen J. Tumor Cell Senescence Response Produces Aggressive Variants. Cell Death Discovery 2017, 3, 17049. [PubMed: 28845296]

(64). Kirkland JL; Tchkonia T. Cellular Senescence: A Translational Perspective. EBioMedicine 2017, 21, 21–28. [PubMed: 28416161]

(65). Watanabe S; Kawamoto S; Ohtani N; Hara E. Impact of Senescence-Associated Secretory Phenotype and its Potential as a Therapeutic Target for Senescence-Associated Diseases. Cancer Sci. 2017, 108 (4), 563–569. [PubMed: 28165648]

(66). Ekpenyong-Akiba AE; Canfarotta F; Abd H B; Poblocka M; Casulleras M; Castilla-Vallmanya L; Kocsis-Fodor G; Kelly ME; Janus J; Althubiti M; Piletska E; Piletsky S; Macip S. Detecting and Targeting Senescent Cells using Molecularly Imprinted Nanoparticles. Nanoscale Horizons 2019, 4, 757–768.

(67). Li Y; Hou X; Yang C; Pang Y; Li X; Jiang G; Liu Y. Photoprotection of Cerium Oxide Nanoparticles against UVA radiation-induced Senescence of Human Skin Fibroblasts due to their Antioxidant Properties. Sci. Rep 2019, 9 (1), 2595. [PubMed: 30796322]

(68). Baetke SC; Lammers T; Kiessling F. Applications of Nanoparticles for Diagnosis and Therapy of Cancer. Br. J. Radiol 2015, 88 (1054), 20150207.

(69). Furler RL; Nixon DF; Brantner CA; Popratiloff A; Uittenbogaart CH TGF-beta Sustains Tumor Progression through Biochemical and Mechanical Signal Transduction. Cancers 2018, 10 (6), 199.

(70). Demaria M; O'Leary MN; Chang J; Shao L; Liu S; Alimirah F; Koenig K; Le C; Mitin N; Deal AM; Alston S; Academia EC; Kilmarx S; Valdovinos A; Wang B; de Bruin A; Kennedy BK; Melov S; Zhou D; Sharpless NE; Muss H; Campisi J. Cellular Senescence Promotes Adverse Effects of Chemotherapy and Cancer Relapse. Cancer Discovery 2017, 7 (2), 165–176. [PubMed: 27979832]

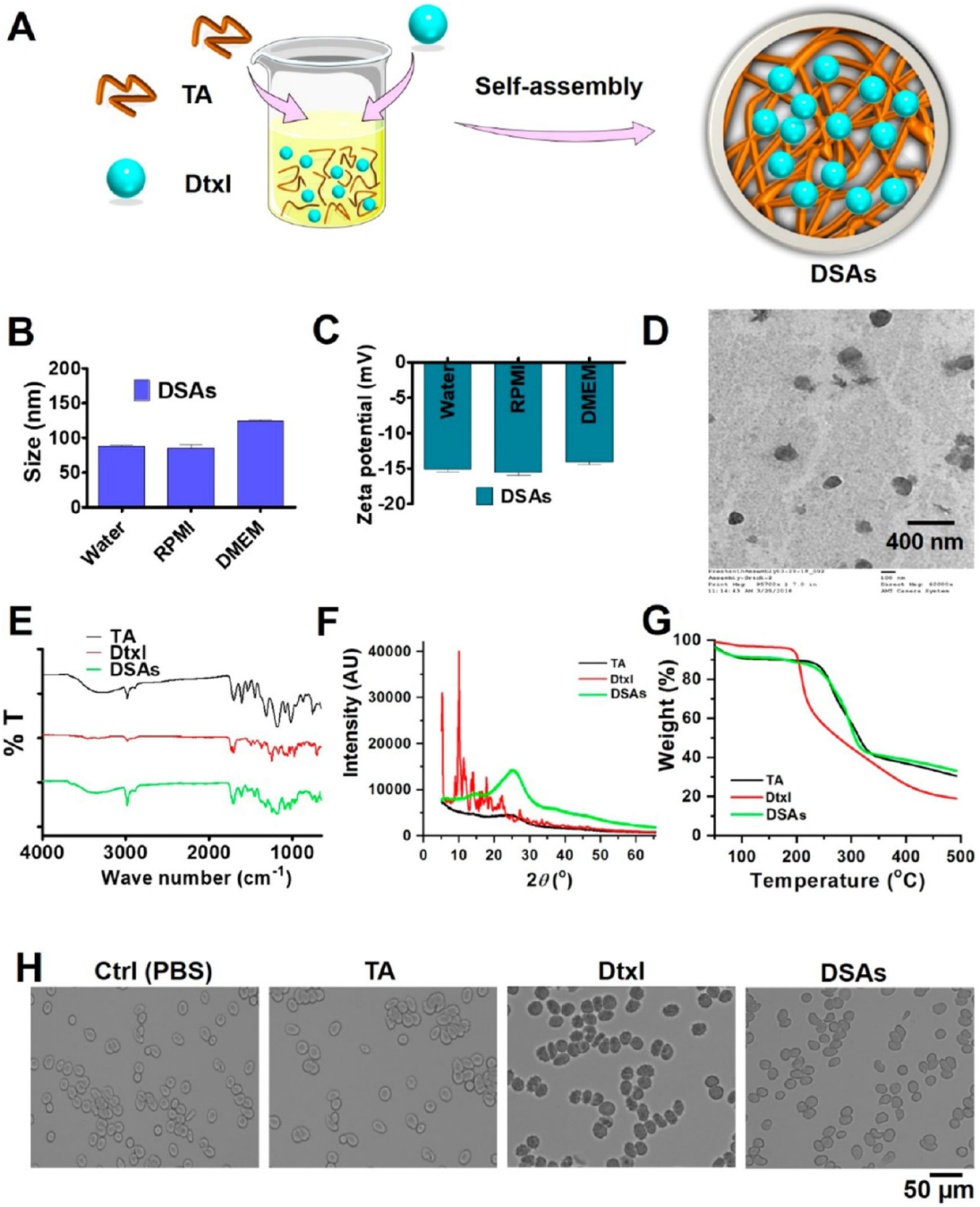

Figure 1.

Preparation and characterization of Tannic acid-Docetaxel self-assemblies (DSAs). (A) Schematic representation of DSAs preparation. (B-H) Characterization studies of DSAs. (B) Size distribution, (C) Zeta potential, (D) TEM, (E) FT-IR, (F) XRD, and (G) TGA. (H) Qualitative hemolytic studies of DSAs (morphological).

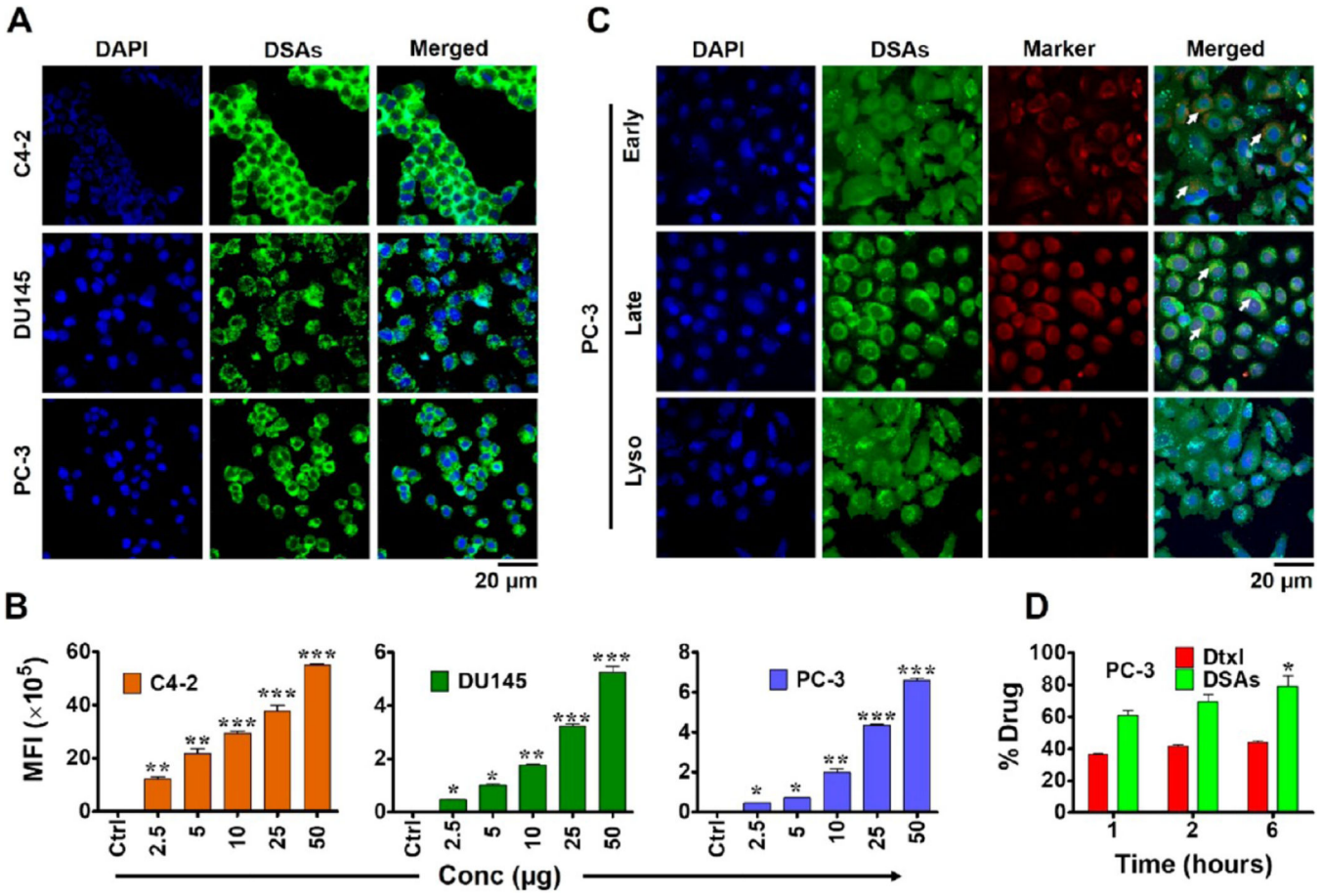

Figure 2.

Intracellular uptake behavior of DSAs in prostate cancer cells. (A) Cellular uptake of DSAs formulation labeled with fluorescence tag (Coumarin 6) in C4–2, DU145, and PC-3 prostate cancer cells after 3 h incubation. (B) Quantitative analysis of DSAs cellular uptake in C4–2, DU145, and PC-3 cells by flowcytometric studies. (C) Endosomal escape studies of C-6 labeled DSAs in PC-3 cells. The cells were labeled with endosomal (transferrin-Early; Rab7a-Late) and lysosomal (Red DND-99) markers, where DSAs was incubated for 3 h. (D) Assessment of DSA uptake in PC-3 cells by validating the intracellular drug content through LC-MS/MS after nanoformulation treatment for 1, 2, and 6 h. Cells were exposed to DSAs (equivalent to 500 ng of Dtxl) resulting in 79.15% of intracellular drug release in 6 h. Representative images were captured at 40× magnification. All statistical analysis was performed using a student's *t* test. Bars represent mean ± SEM. *, **, and *** represent the level of significance with *P* (<0.05, 0.01, and 0.001) with respect to control.

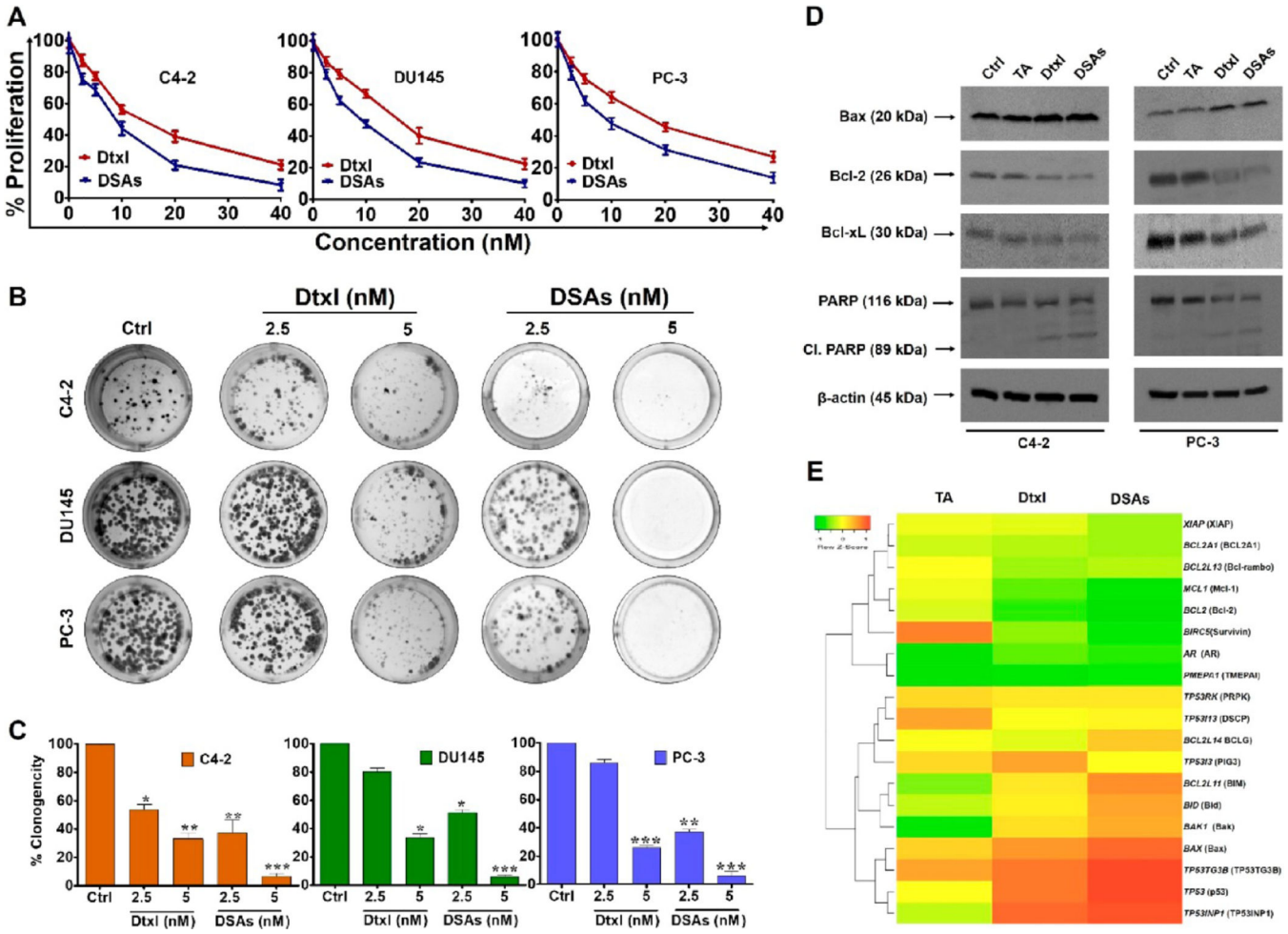

Figure 3.

Enhanced *in vitro* anticancer effects of DSAs in prostate cancer cells. (A) Cell proliferation measured by MTS assay. Exposure to DSAs distinctly reduced C4–2, DU145, and PC-3 prostate cancer cell proliferation. Cells were treated with 1−40 nM DSAs and equivalent Dtxl for 48 h and measured by for absorbance at 490 nm after MTS treatment. (B) DSAs effectively inhibits the clonogenic potential of C4–2, DU145, and PC-3 cells. The treatments were subjected at 2.5 and 5 nM of Dtxl and DSAs (Dtxl equivalent) for 7 days. After the treatments, culture medium containing drug were replace with drug free medium and allowed to grow for 7 days, processed and visualized. (C) Colony number was counted after treatments and graphically represented. Here, the control cells were considered as 100% clonogenicity. (D) DSAs induce proapoptotic signaling in C4–2 and PC-3 prostate cancer cells. Immunoblot analysis of cell lysates treated with TA, Dtxl, and DSAs were probed with proteins related apoptotic signaling. (E) Gene expression of apoptotic signaling related proteins in C4–2 cells after TA, Dtxl, and DSAs (Dtxl equivalent) treatments through heat map analysis. Data presented as mean ± standard error of the mean ($n = 3$); each performed in triplicate. All statistical analysis was performed using student's t test. Bars represent mean ± SEM. *, **, and *** represent the level of significance with P (<0.05, 0.01, and 0.001) with respect to control.

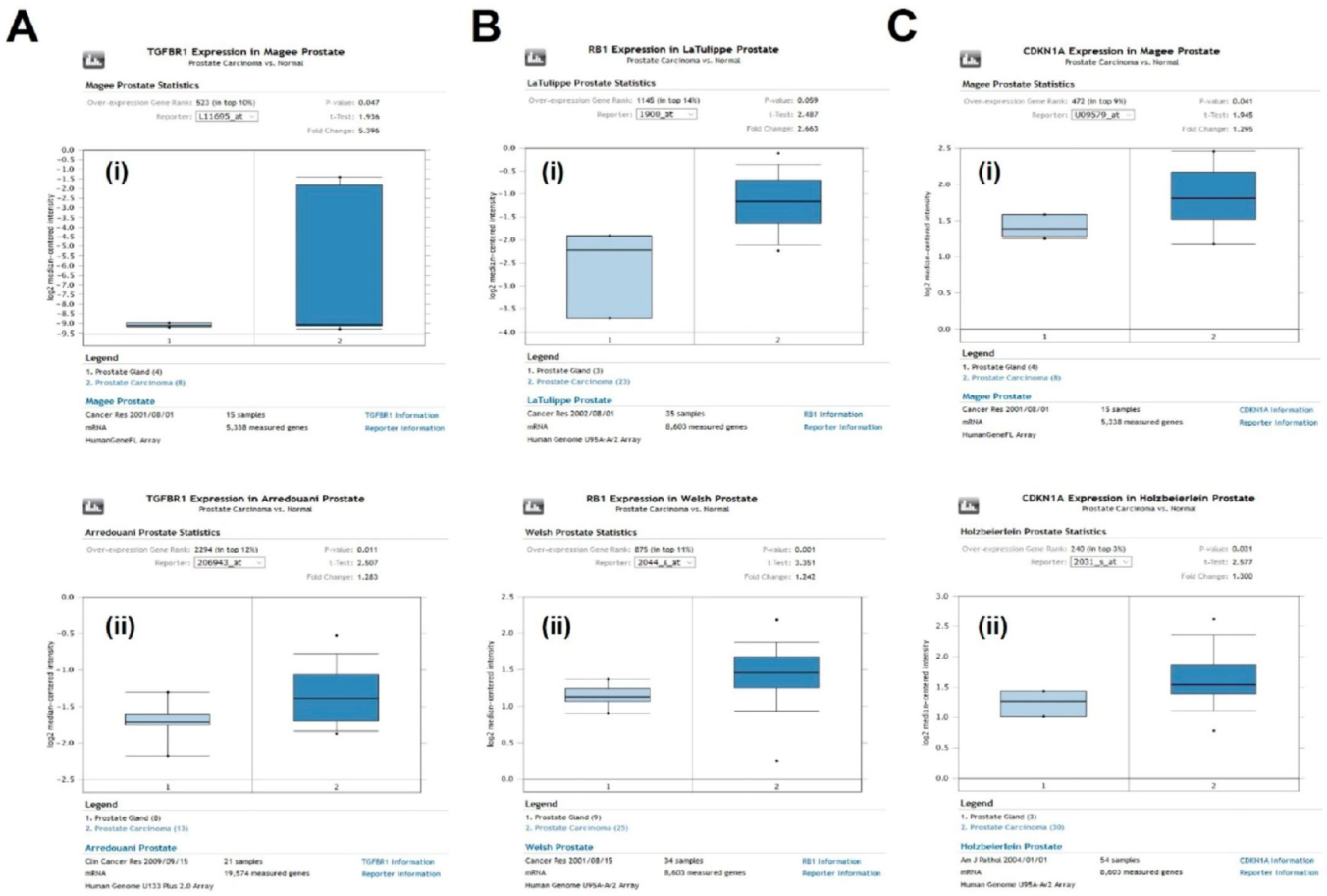

Figure 4.

Expression of senescence biomarkers in prostate cancer and normal samples curated from the *ONCOMINE* database: (A) TGFβR1 expression (i and ii), (B) RB1 (Rb, i and ii), and (C) CDKN1A (p21, i and ii).

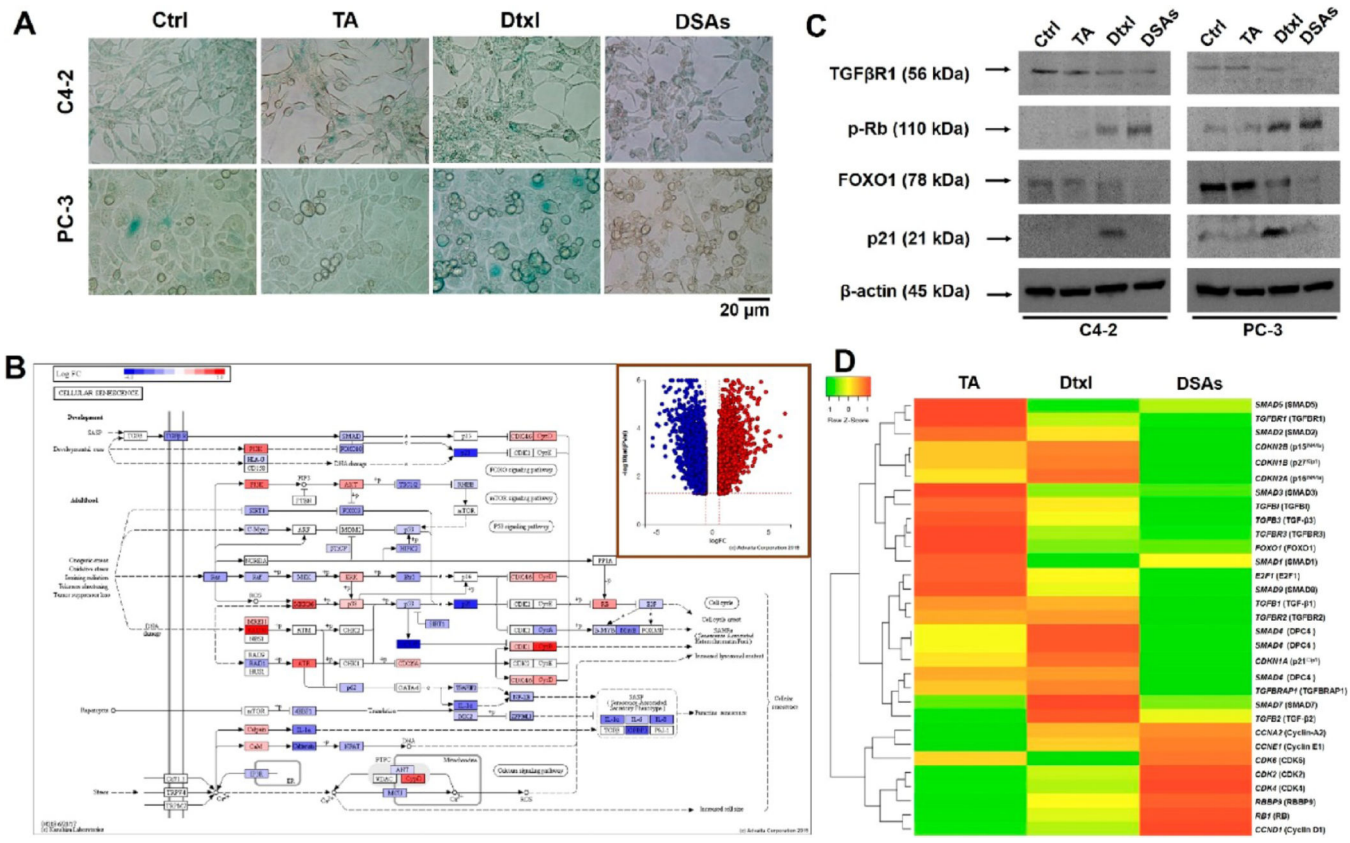

Figure 5.

DSAs blockage of senescence in prostate cancer cells. (A) Senescence-associated β-galactosidase activity in C4–2 and PC-3 cells treated with TA, Dtxl, and DSAs assessed by X-gal staining. Representative images are shown with representative X-gal-positive cells. (B) Molecular inhibition of senescence signaling by DSAs in PC-3 cells through iPathwayGuide analysis. (inset) Volcano plot of 5235 differentially expressed genes. (C) DSAs interfere with senescence associated with TGFβR1/FOXO1/p21 signaling axis in both C4–2 and PC-3 cells. (D) Heat map analysis of senescence associated genes through microarray studies in PC-3 cells treated with TA, Dtxl, and DSAs. Data presented as mean ± standard error of the mean (n = 3); each are performed in triplicate.

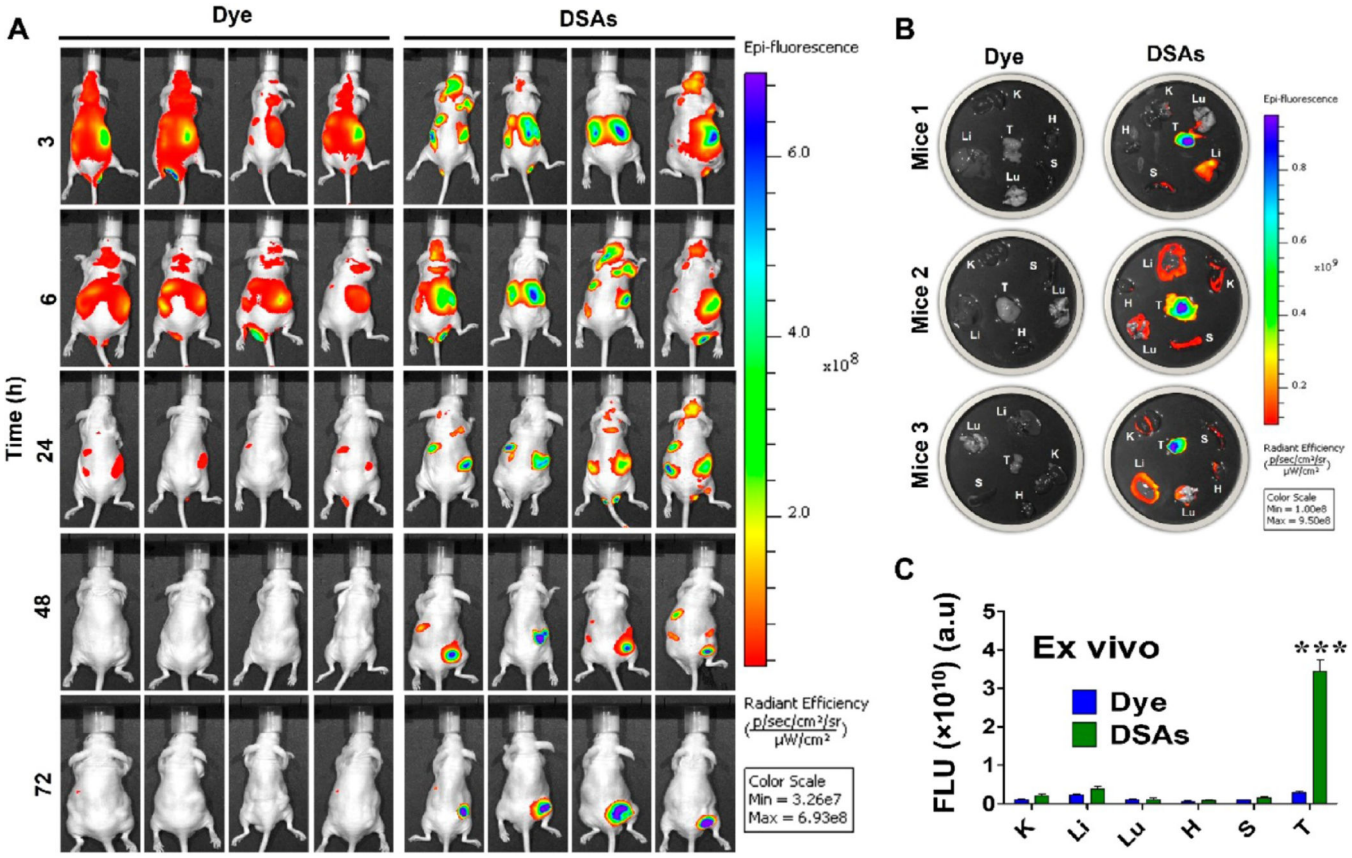

Figure 6.

Tumor targeting ability of DSAs. (A) *In vivo* fluorescent imaging of mice bearing PC-3 xenograft tumors treated with dye (free ICG) and ICG-DSAs. The mice treated with dye and ICG labeled DSAs were imaged using the IVIS Lumina XRMS *in vivo* imaging system at various time intervals (3, 6, 24, 48, and 72 h). (B) *Ex vivo* imaging of tumors and organs obtained from euthanized mice treated with dye and ICG-DSAs after 72 h. (C) Quantitative *ex vivo* analysis of the fluorescence signals of tumor and major organs (kidney K, liver Li, lung Lu, heart H, spleen S, tumor T) obtained from mice treated with dye and ICG-DSAs after the euthanization process. All statistical analysis was performed using a student's *t* test. Data is presented as mean ± standard error of the mean $n = 4$ for *in vivo* and $n = 3$ for *ex vivo* imaging.

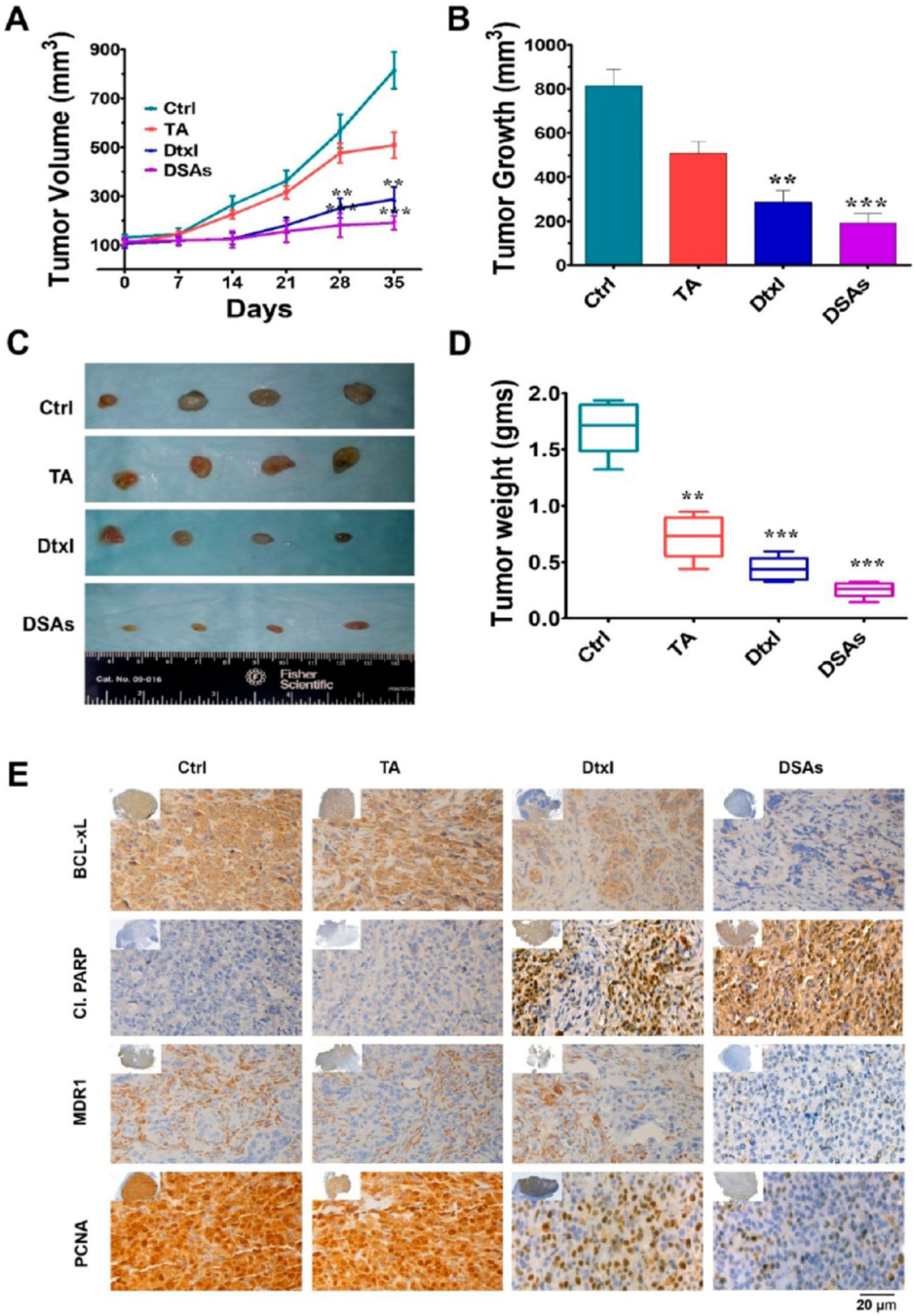

Figure 7.

Antitumor activity of DSAs in PC-3 human prostate carcinoma xenografts. Effect of TA, Dtxl, and DSAs on PC-3 cell derived xenograft tumors in athymic nude mice: (A) tumor volume; (B) net tumor growth; (C) excised tumor images of treated mice; (D) tumor weights; (E) IHC of TA, Dtxl, and DSAs treated PC-3 human prostate carcinoma xenografts. DSAs treatments blockade the senescence related TGFβR1/p21 axis and activate apoptotic signaling in PC-3 tumors. Paraffin-embedded sections of PC-3 bearing tumors in nude mice were processed and IHC was done. IHC of Bcl-xL, Cl-PARP, MDR, and PCNA,

representative of three independent experiments. Representative images were captured at 40× magnification. Data presented as mean ± standard error of the mean ($n = 8$), each performed in triplicate. All statistical analysis was performed using student's t test. Bars represent mean ± SEM. ** and *** represent the level of significance with P (<0.01 and 0.001) with respect to control.

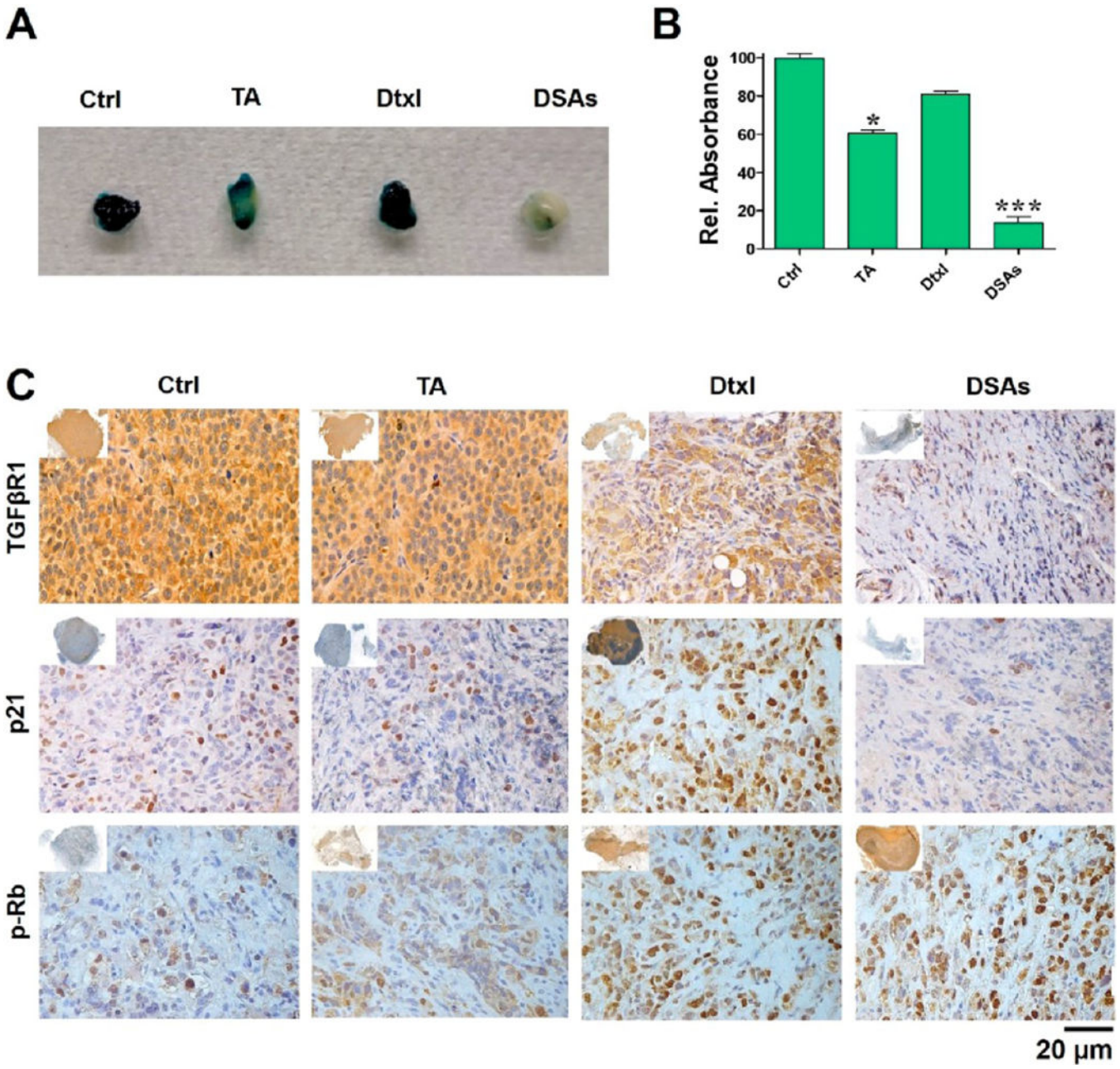

Figure 8.

Antisenescence activity of the DSAs in PC-3 human prostate cancer xenografts. (A) β-galactosidase staining of the excised tumor tissues (20 mg) obtained from mice treated with vehicle, TA, Dtxl, and DSAs. The tissues were subjected to staining overnight and incubated at 37 °C in the staining solution. (B) Relative absorbance of the tissue incubated staining solutions. The absorbance of the staining solution was measured for absorbance maxima at 650 nm. (C) Senescence associated regulatory proteins (TGFβR1, p21, and Rb) was evaluated in xenograft tumors by IHC studies. The images were captured at 40× magnification. Data presented as mean ± standard error of the mean (n = 4), each performed in triplicate. All statistical analysis was performed using student's t test. Bars represent mean

± SEM. * and *** represent level of significance with P (<0.05 and 0.001) with respect to control.

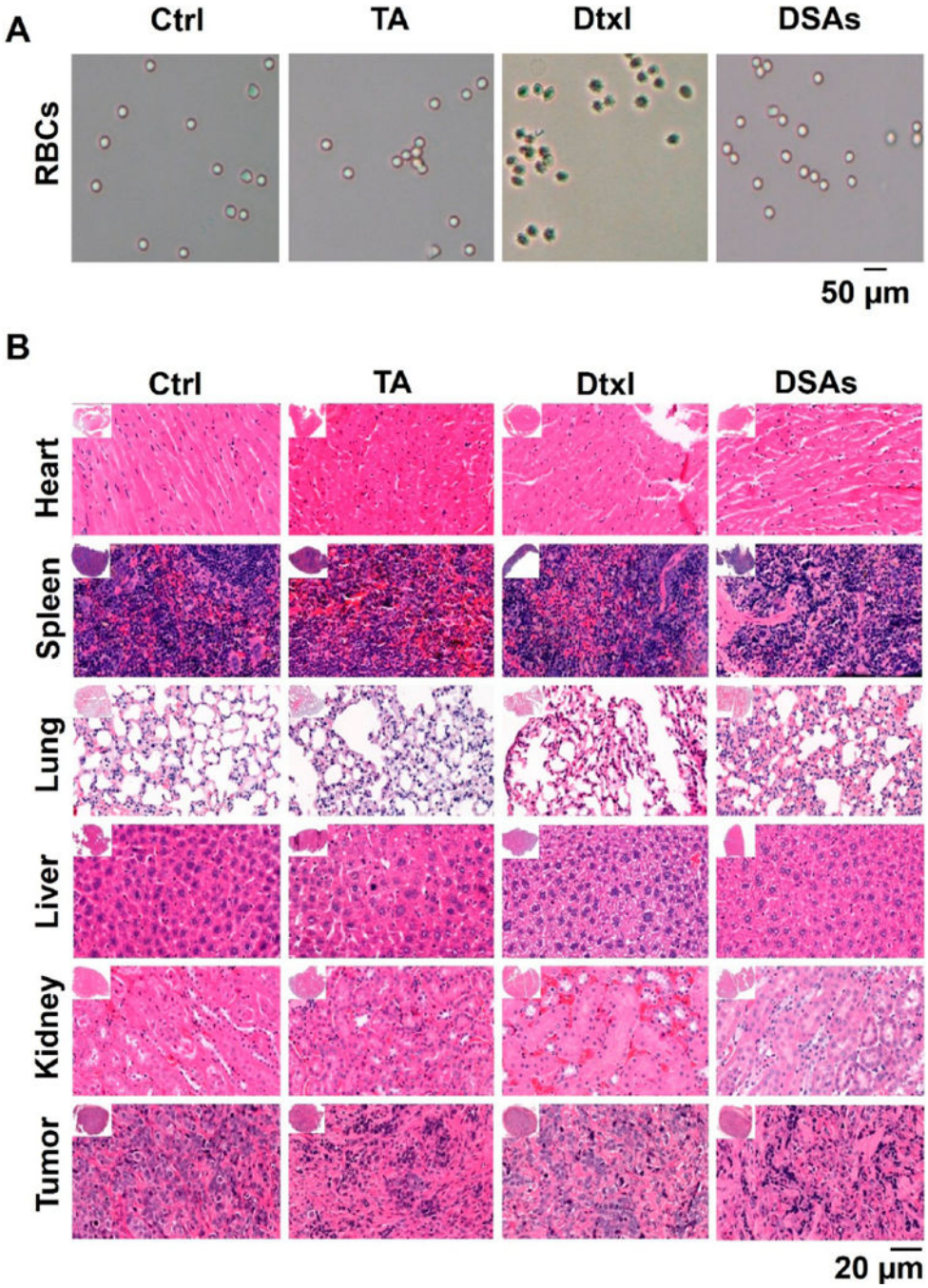

Figure 9.

Biocompatible and toxicity studies of DSAs. Hemolytic assay. (A) Representative images of RBC morphology of mice blood treated with vehicle, TA, Dtxl, and DSAs. (B) H&E staining of organs (heart, spleen, lung, liver, and kidney) and tumors of mice treated with TA, Dtxl, and DSAs.

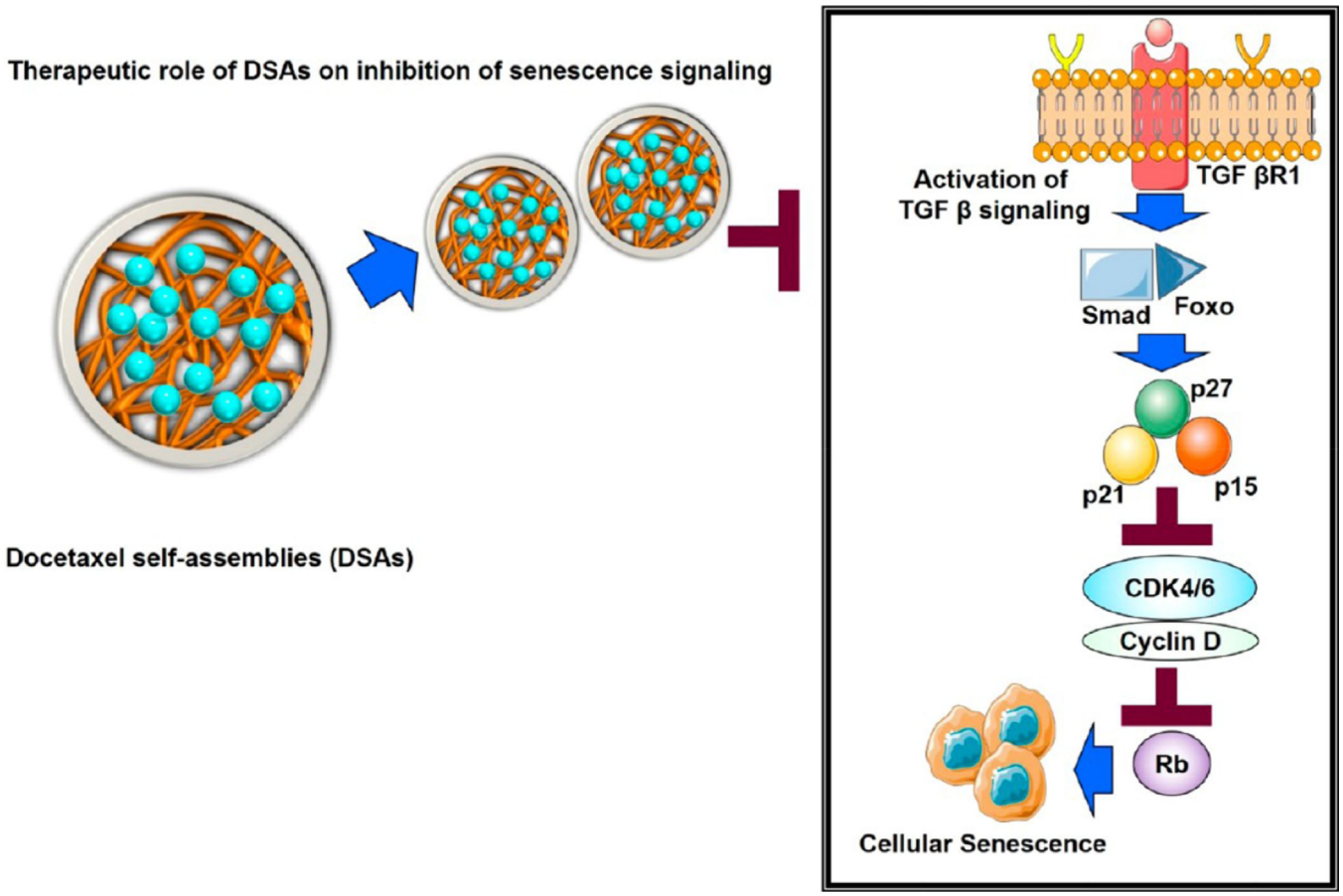

Figure 10.
Antisenescence mechanism of action by DSAs formulation in prostate cancer.

Table 1.

Serum Analysis of Enzymes Related to Hepatic and Kidney Functions in Mice after the Treatments[a]

ID normal ranges	Alb g/dL 2.5–3.5	ALP U/L 35–96	ALT U/L 17–77	AST U/L 54–298	BUN mg/dL 8–33	Ca mg/dL 7.1–10.1	Creat mg/dL 0.2–0.9	Glu mg/dL 62–175	TBili mg/dL 0.0–0.9	TP g/dL 3.5–7.2
Ctrl	3.40 ± 0.10	53.33 ± 11.69	41.33 ± 2.33	106.66 ± 9.73	26.66 ± 1.76	11.20 ± 0.70	0.76 ± 0.20	136.00 ± 11.00	0.16 ± 0.03	7.30 ± 0.30
TA	3.36 ± 0.08	73.33 ± 12.54	60.33 ± 8.64	172.66 ± 13.93	24.66 ± 1.20	09.66 ± 0.16	0.80 ± 0.05	095.66 ± 09.13	0.20 ± 0.05	5.96 ± 0.16
Dtxl	3.30 ± 0.15	77.33 ± 3.17	101 ± 44.06	157.00 ± 59.00	25.66 ± 0.88	10.46 ± 0.72	0.63 ± 0.17	088.33 ± 16.22	0.20 ± 0.00	6.86 ± 0.34
DSAs	3.36 ± 0.08	52.66 ± 2.72	61.66 ± 4.84	123.33 ± 14.15	24.66 ± 1.45	09.73 ± 0.03	0.43 ±0.18	124.33 ± 19.34	0.33 ± 0.08	6.30 ± 0.45

[a]**AST:** aspartate aminotransferase. **ALT:** alanine aminotransferase. **ALP:** alkaline phosphatase. **TP:** total protein. **Tbili:** total bilirubin. **Alb:** albumin. **Create:** creatinine; **BUN:** blood urea nitrogen. **Ca:** calcium; **Glu:** glucose.